Journal of Materials Chemistry A

ROYAL SOCIETY OF CHEMISTRY

REVIEW

View Article Online
View Journal | View Issue

Cite this: J. Mater. Chem. A, 2025, 13, 12009

Optimization strategies for flexible aqueous rechargeable sodium-ion batteries (ARSIBs)

Hehe Ren, Xinzhan Du, Jing Liang* and Wei Wu *

Flexible aqueous rechargeable sodium-ion batteries (ARSIBs) have emerged as promising energy storage systems for flexible and wearable electronics due to their safety, eco-friendliness, flexibility, and low cost, especially for large-scale and high-throughput storage needs. However, the design of flexible ARSIBs with high performance and excellent mechanical performance still faces challenges including the structural stability of electrodes, narrow electrochemical stability window of electrolytes, various side reactions, and structural design. It is urgent to design and develop ARSIBs with superior electrochemical performance, excellent mechanical performance and broader application scenarios. While there have been numerous reviews on sodium-ion batteries, there is a scarcity of exclusive reviews focusing on flexible ARSIBs. This review systematically introduces the advancements in electrode materials, electrolytes, and their optimization strategies for flexible ARSIBs. In addition, the recent advancements of batteries are discussed in terms of design strategies, multifunctional applications, and damage resistance. To manufacture flexible ARSIBs with coordinated high energy density and multi-functionality, not only the active materials and electrolytes should be optimized, but also the structural design should be improved. This review aims to evaluate the challenges and future prospects, and offer valuable references for designing advanced and high-performance flexible ARSIBs.

Received 11th January 2025
Accepted 19th March 2025

DOI: 10.1039/d5ta00276a

rsc.li/materials-a

1. Introduction

In view of the success of flexible and wearable electronics, urgently developing an energy storage system with safety and flexibility has become a top priority. Since their commercialization in 1991, lithium-ion batteries (LIBs) have been widely used in portable electronics (such as watches, mobile phones, cameras, and computers), as well as automotive applications.[1–5] Although conventional LIBs offer high energy density, their rigid nature, safety issues, limited lithium resources, and high costs remain unavoidable, hindering their further development in the fields of wearable electronics and foldable flexible electronics. Due to the advantages of eco-friendliness, flexibility and abundant sodium resources, flexible aqueous rechargeable sodium-ion batteries (ARSIBs) have greater market competitiveness in the development of portable flexible electronics.[6–11]

During the charging process of flexible ARSIBs, Na^+ migrates from the cathode to the anode *via* the electrolyte, while

Laboratory of Printable Functional Materials and Printed Electronics, School of Physics and Technology, Wuhan University, Wuhan 430072, PR China. E-mail: jingliang@whu.edu.cn; weiwu@whu.edu.cn; Fax: +86-27-68778491; Tel: +86-27-68778491

Hehe Ren

Hehe Ren is currently pursuing her Ph.D. in the School of Physics and Technology at Wuhan University under the supervision of Prof. Wei Wu. Her current research interests mainly focus on the synthesis of electrochemical materials and their applications in flexible sodium-ion batteries.

Xinzhan Du

Xinzhan Du is currently studying for her Master's degree in the School of Physics and Technology at Wuhan University under the supervision of Prof. Wei Wu. Her current research includes the fabrication of nanomaterials and their applications in flexible supercapacitors.

electrons flow from the cathode to the anode through the external circuit, often accompanied by redox reactions (Fig. 1). Therefore, the development of active materials and electrolytes has received increasing attention in recent years. However, unlike non-aqueous systems, aqueous batteries encounter special challenges, including the limited electrochemical stability window (ESW) of water (1.23 V) and irreversible side reactions involving the hydrogen evolution reaction (HER), oxygen evolution reaction (OER), and proton co-insertion. The above problems not only lead to low coulomb efficiency (CE), poor cycling performance, and low energy density, but also cause battery bloating/expansion. Therefore, designing and preparing suitable active materials and electrolytes are essential for high-performance flexible ARSIBs.

The Na/S battery with metallic sodium as anode and elemental sulfur as cathode is the earliest sodium battery in the world.[12] Subsequently, people began to explore the electrochemical behavior of Na^+ in aqueous electrolytes, as well as the structural design of flexible aqueous batteries to obtain safe and environmentally friendly flexible ARSIBs.[13–17] Fig. 2 shows the evolution of flexible ARSIBs from 2017 to 2024.[18–24] The electrochemical performance and applications of flexible ARSIBs including fiber-based, paper-based, metal current collector-based, and self-supporting ARSIBs were further explored.[25–27] The above studies have demonstrated the potential of flexible ARSIBs as promising energy storage systems in wearable and implantable electronics fields.

This review offers an overview of the most recent research progress in flexible ARSIBs, including battery constituent components, structural design strategies, and practical applications. Firstly, we introduce the developments of active materials in ARSIBs, and summarize the optimization and

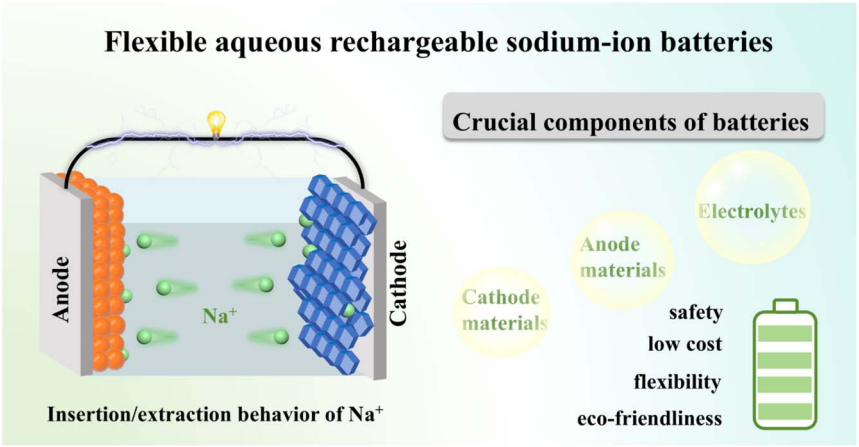

Fig. 1 The mechanism and crucial components of flexible ARSIBs.

Jing Liang

Jing Liang received her Ph.D. degree from Wuhan University under the supervision of Prof. Wei Wu in 2021. Currently, she is conducting her postdoctoral research at Materials Processing Engineering of Wuhan University. Her research interest is focused on printed electronics, and electrochemical materials and their flexible energy storage applications, including supercapacitors and batteries.

Wei Wu

Wei Wu received his Ph.D. degree from Wuhan University in 2011. He then joined the group of Prof. Daiwen Pang at Wuhan University (2011) and Prof. V. A. L. Roy at the City University of Hong Kong (2014) as a postdoctoral fellow. Currently, he is a full professor of the School of Physics and Technology, Wuhan University. He received National Award for Excellence in Innovation in 2023, 15th Bi Sheng Award of Printing Technology in 2019, STAM Best Paper Award in 2017 and Hong Kong Scholars Award in 2014. He has published over 100 papers, which have received over 15 000 citations. His research interests include the synthesis and application of printable functional materials, printed electronics, wearable electronics and intelligent packaging, flexible sensors and related systems.

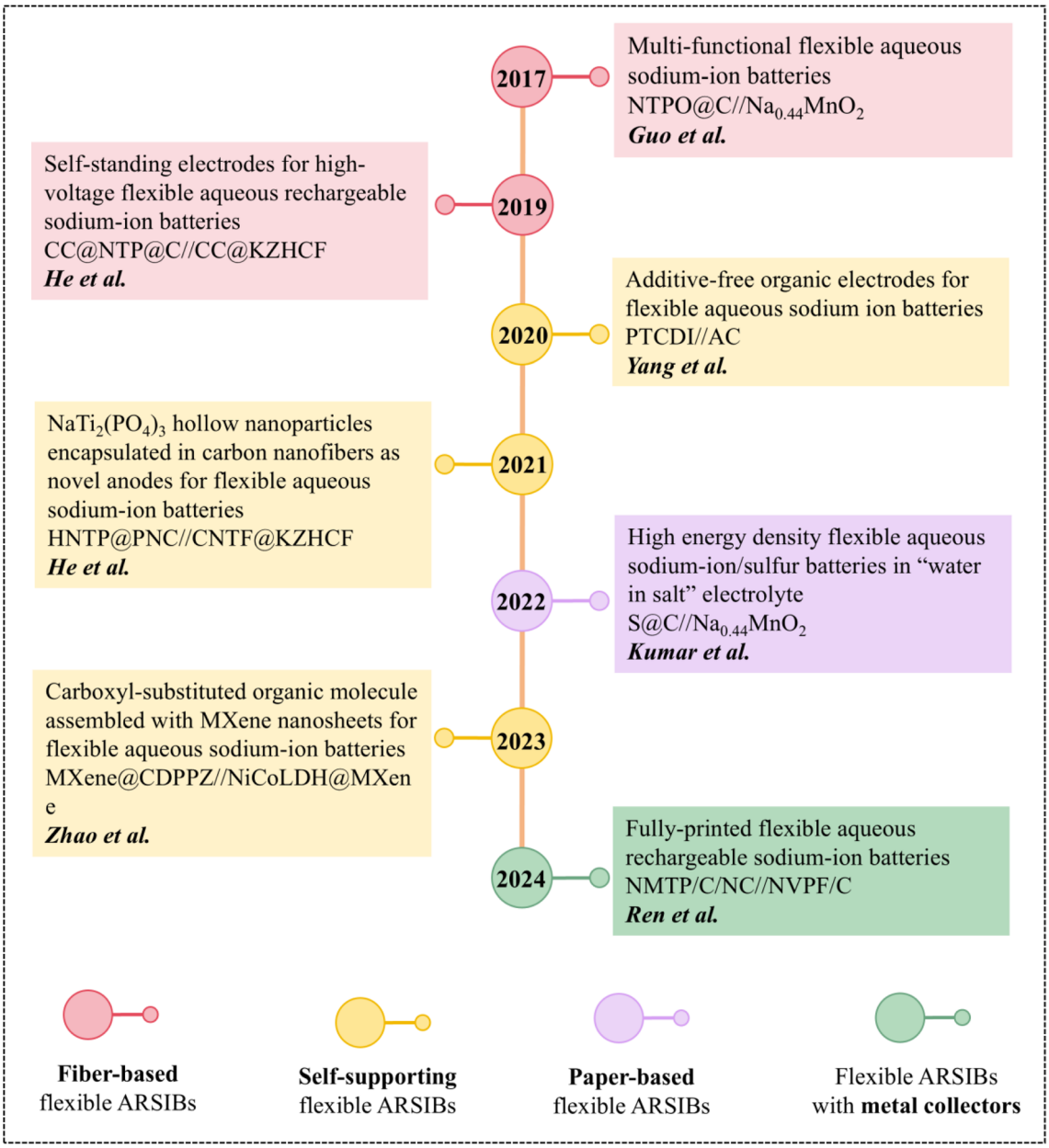

Fig. 2 The major development of flexible ARSIBs with different structural designs in recent years.[18–24]

improvement strategies, aiming at enhancing the electrochemical performance of active materials. Secondly, we systematically discuss diluted/concentrated electrolytes, low freezing point electrolytes, and hydrogel electrolytes in ARSIBs. Our findings suggest that utilizing optimized electrolytes could potentially alleviate the limitations of certain electrode materials, thereby enhancing their electrochemical performance. And then, according to the structural design, we elucidate advanced configurations for flexible ARSIBs, such as fiber-based, paper-based, metal current collector-based, and self-supporting ARSIBs. Then the adaptability of flexible ARSIBs in practical applications and their stability under extreme conditions are discussed. Finally, we briefly discuss the future prospects and challenges for flexible ARSIBs. To manufacture flexible ARSIBs with coordinated energy density and functionality, it is crucial to optimize active materials and electrolytes, and improve structural design strategies. The purpose of this review is not only to summarize the development and applications of flexible ARSIBs, but also to provide comprehensive information on flexible ARSIBs.

2. Cathode materials and optimization strategies

Compared with conventional LIBs, ARSIBs hold great potential as next-generation energy storage devices due to their abundant sodium resources and aqueous electrolytes, which meet the

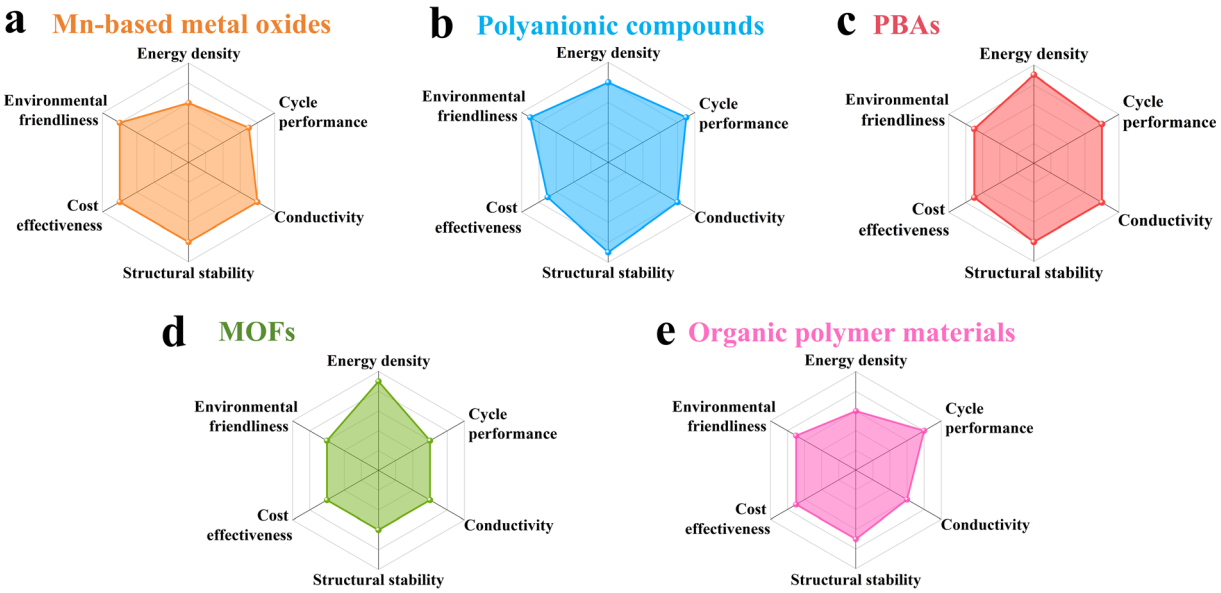

Fig. 3 Performance comparison of (a) Mn-based oxides, (b) polyanionic compounds, (c) PBAs, (d) MOFs, and (e) organic polymer materials.

requirements of safety, low cost, and environmental friendliness. Currently, the active materials used for the cathodes of ARSIBs primarily include Mn-based oxides, polyanionic compounds, Prussian blue analogues (PBAs), metal organic frameworks (MOFs), and organic polymer materials. Fig. 3 provides a performance comparison of these cathode materials, including energy density, cycle performance, conductivity, structural stability, cost effectiveness, and environmental friendliness. In the following sections, we will specifically discuss the performance of cathode materials and optimization strategies, providing valuable insights for the development of high-performance ARSIBs.

2.1. Cathode materials

2.1.1. Mn-based metal oxides. Transition metal oxides are attractive cathode materials for various energy storage systems, due to their appealing capacity, facile manufacturing processes and excellent stability. Transition metal oxides like V_2O_5, MnO_2, and RuO_2 are frequently utilized as cathode materials of ARSIBs. However, these metal oxides primarily exhibit capacitive behavior, involving Faraday adsorption and desorption processes on their surface, rather than insertion/extraction behaviors of Na^+ or chemical reactions.[28–30]

MnO_2 exhibits a representative pseudocapacitance behavior in the neutral electrolyte.[31] Moreover, the insertion of Na^+ into MnO_2 will induce an irreversible phase, which limits the wide applications of MnO_2 in ARSIBs.[32] In recent years, Na_xMnO_2 compounds have been considered promising cathode materials in ARSIBs, which have recently attracted major attention. A variety of Na_xMnO_2 sodium compounds were synthesized with different sodium to manganese ratios, such as $Na_{0.27}MnO_2$, $Na_{0.40}MnO_2$, and $Na_{0.44}MnO_2$. It has been demonstrated that $Na_{0.44}MnO_2$ undergoes a biphasic reaction involving Na^+ intercalation, different from the capacitive behavior of MnO_2 in aqueous electrolytes (Fig. 4a).[33] After charging/discharging for 1000 cycles, the $Na_{0.44}MnO_2$ cathode still exhibits excellent electrochemical performance, and the capacity of $Na_{0.44}MnO_2$ can reach 35 mA h g^{-1} (0.5 A g^{-1}). Subsequently, a sodium rich disordered birnessite $Na_{0.27}MnO_2$ exhibits excellent discharge capacity (138 mA h g^{-1}), high energy efficiency, and appealing cycle performance, as well as nearly 100% CE after 5000 cycles (Fig. 4b).[34] In summary, various Na_xMnO_2 compounds are developed as potential cathodes in ARSIBs, and their crystal structures and properties depend on the ratio of sodium. Nevertheless, these materials present significant volume shrinkage/expansion throughout the charging/discharging process, resulting in structural collapse and rapid capacity reduction.

2.1.2. Polyanionic compounds. $Na_xM_y(XO_4)_n$ (X = S, P, Si, As, Mo and W; M = transition metal elements) polyanionic compounds exhibit an open framework structure, which includes the tetrahedral anion units $(XO_4)_n^-$ and MO_x polyhedra with strong covalent bonds.[35] This unique framework structure of polyanionic compounds facilitates the rapid transfer of Na^+, enhances the active sites of materials, leading to high capacity and excellent cycle performance. Among them, $NaFePO_4$, $Na_3V_2(PO_4)_3$ (NVP) and their derivatives are regarded as attractive cathodes for ARSIBs, owing to their wide channel structure, stability and large surface area.

Olivine-type $LiFePO_4$ is widely used in LIBs due to its stable structure and appealing energy density. The sodium-rich polyanionic compound $NaFePO_4$ is extensively investigated as an active material for ARSIBs, presenting a similar structure to $LiFePO_4$. As shown in Fig. 4c, the open framework structure of $NaFePO_4$ is formed by the sharing of a side and corners between the PO_4^{3-} tetrahedron and the FeO_6 octahedron.[36] $NaFePO_4$ provides high theoretical capacity (154 mA h g^{-1}) and a wide ESW of 2.8 V, due to the existence of the Fe^{3+}/Fe^{2+} redox couple.

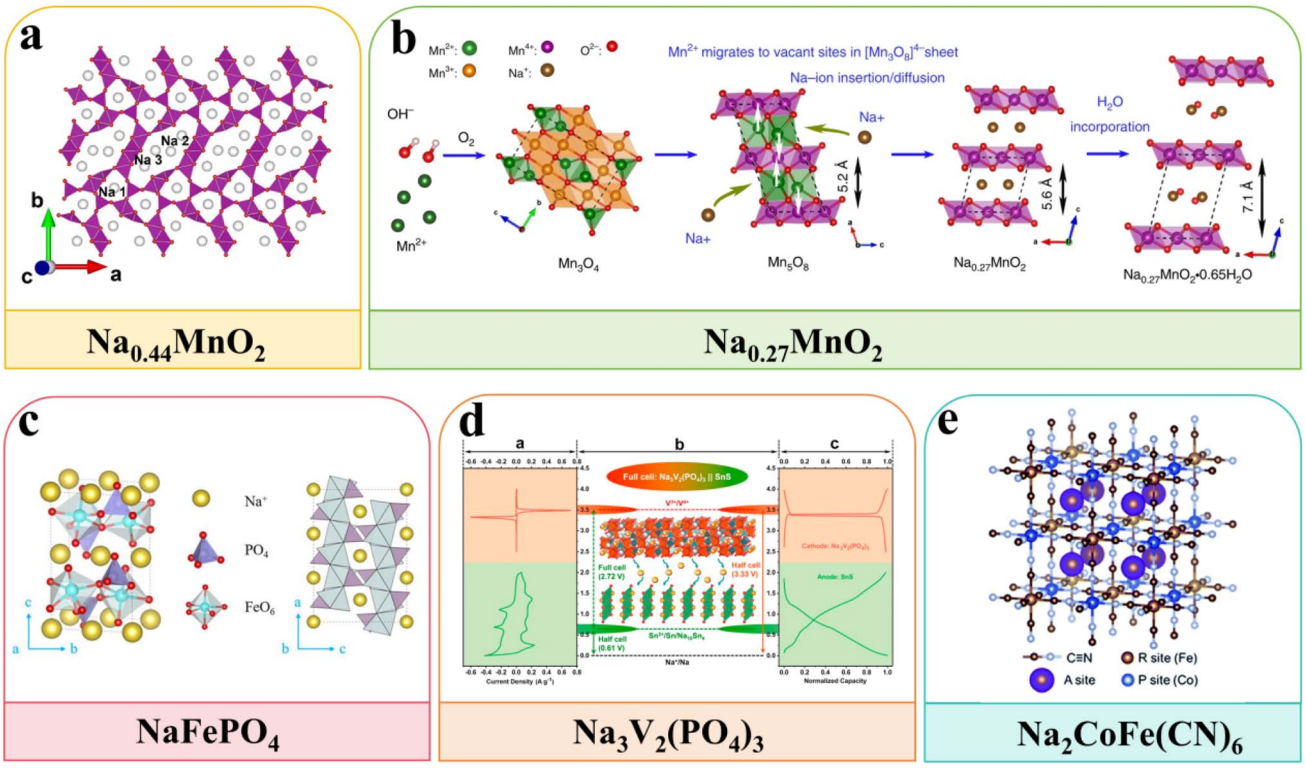

Fig. 4 Schematic illustration of the crystal structure of (a) $Na_{0.44}MnO_2$,[33] reproduced from ref. 33 with permission from Elsevier, copyright 2019. (b) $Na_{0.27}MnO_2$,[34] reproduced from ref. 34 with permission from Springer Nature, copyright 2019. (c) $NaFePO_4$,[36] reproduced from ref. 36 with permission from the American Chemical Society, copyright 2020. (d) $Na_3V_2(PO)_4$,[37] reproduced from ref. 37 with permission from Elsevier, copyright 2019 and (e) $Na_2CoFe(CN)_6$.[46]

As shown in Fig. 4d, the framework structure of NVP is made up of sharing corners between three PO_4 tetrahedra and a VO_6 octahedron, which creates a large interstitial space and a three-dimensional (3D) network of interconnected channels to facilitate the insertion/extraction behaviors of Na^+. The NVP presents high theoretical capacity and appealing stability, due to the multivalent redox reaction of V^{2+}/V^{5+} redox couples and the strong V–P bonds. The $Na_3V_2(PO_4)_3$/C (NVP/C) with 3D framework structure is prepared by electrospinning technology, which presents phenomenal discharge capacity (101 mA h g^{-1}), outstanding electrochemical performance and great stability.[37] However, polyanionic compounds still face the following challenges: (1) the inherent low conductivity, (2) the instability of electrode materials in aqueous electrolytes. These problems lead to poor cycle performance and limit the practical applications of polyanionic compounds.

2.1.3. PBAs. The typical framework structure of PBAs is represented by the chemical composition $A_nM_1[M_2(CN)_6]_m \cdot xH_2O$ ($0 \le n \le 2$, $0 \le m \le 1$, $0 \le x$), where A represents alkali metals or alkaline earth metal ions and M_1 and M_2 represent transition metal ions (Fe, Mn, Ni, Co, Mo, and Cu ions).[38–41] And the Fe^{3+}/Fe^{2+} redox couple and other transition metal ion redox couples provide a high ESW and excellent capacity. These materials are regarded as ideal cathode materials for ARSIBs, owing to the 3D framework structure, excellent theoretical capacity, and eco-friendliness. PBAs with open framework structure and 3D channels enable rapid ion diffusion, demonstrating excellent cycling stability during the insertion/extraction process of Na^+. Based on their central ion, crystal water, ligand, and outside conditions, PBAs are mainly divided into monoclinic, rhombic, cubic and quadrilateral structures. Different amounts of Na^+ and water molecules enter the PBA lattice, the symmetry of the crystal decreases, the crystal phase changes, and the structure is easy to transform into a monoclinic phase and orthorhombic phase. Although PBAs display valuable applications in energy storage systems, the structural evolvement of PBAs is highly significant and complex, the precise mechanism is still unclear during the charging/discharging process.

Prussian blue materials containing only Fe metal ions undergo single-point redox reactions.[42] In recent years, the stability of the PBA structure has been improved by doping other transition metal ions. In particular, NiFe,[43] CuFe,[44] FeFe,[45] CoFe,[46] and MnFe[47] can perform double-site redox reactions, which shows excellent electrochemical performance. The crystal structure of PBAs influences their redox potential, and the different positions of Na^+ in various crystal structures leads to varying electron polarizations. For example, $Na_2CoFe(CN)_6$ (CoHCF) serves as a promising cathode for ARSIBs, which was prepared using a citric acid-assisted co-precipitation method.[46] The addition of Co^{2+} is conducive to control crystallization, thus enhancing the structural stability of CoHCF throughout the

cycle process (Fig. 4e). After charging/discharging 100 times at 2C, the discharge capacity of CoHCF still remains at 100% of the initial capacity. However, there are limited reports regarding PBAs as cathode materials for ARSIBs, due to the inherent instability of PBAs in aqueous electrolytes.

2.1.4. MOFs. Due to the large radius of Na^+, the MOFs with open framework structures, large specific surface area, and tunable pore sizes are promising electrode materials for sodium-ion batteries (SIBs).[48] However, there are limitations in the chemical stability and conductivity of MOFs, which inhibits fully exploiting their advantages as electrode materials. At present, there are efficient solutions: (1) carbon-coated metal oxides with an ordered framework structure can be obtained by the carbonization of MOFs. (2) The carbon-coated metal selenides and sulfur-doped nitrogen carbon are prepared by selenization and vulcanization of MOFs.

As shown in Fig. 5a, the Sn/SnO@C nano-composites are prepared by the reduction of Sn-MOF with H_2, in which SnO nanorods and Sn nanospheres are embedded in the hexagonal carbon framework.[49] As the anode material for SIBs, Sn/SnO@C exhibits a high capacity of 130.1 mA h g^{-1} (2000 mA g^{-1}), excellent rate performance, and appealing cyclability (Fig. 5b). In Fig. 5c, the nitrogen-carbon coated $FeSe_2$ ($FeSe_2$@NC) with spindle nanostructure is fabricated by polymerization, carbonization and selenization of MIL-BBA.[50] The nitrogen-containing carbon layer effectively improves electronic conductivity, provides more active sites, and alleviates volume expansion caused by the Na^+ diffusion process. $FeSe_2$@NC exhibits excellent cycling stability with the capacity of 269.8 mA h g^{-1} after charging/discharging 500 times. As shown in Fig. 5d, the sulfur-doped porous carbon (S/C) is fabricated by carbonization and vulcanization of MOF-5.[51] The ordered framework carbon shows a large specific surface area and provides more active sites, making it an excellent host for sulfur. The unique structure endows the S/C anode with outstanding cycle stability, and the discharge capacity is 268.8 mA h g^{-1} after 100 cycles at 0.1 A g^{-1}. The active materials prepared by carbonization, selenization and vulcanization of MOFs possess phenomenal Na^+ storage capacities. However, the chemical stability of MOFs in aqueous electrolytes is limited, and there are few literature reports on MOFs as electrode materials for ARSIBs.

2.1.5. Organic polymer materials. Organic polymer materials mainly contain elements such as C, H, O, N, and S, which can tailor molecular structures by modifying functional groups

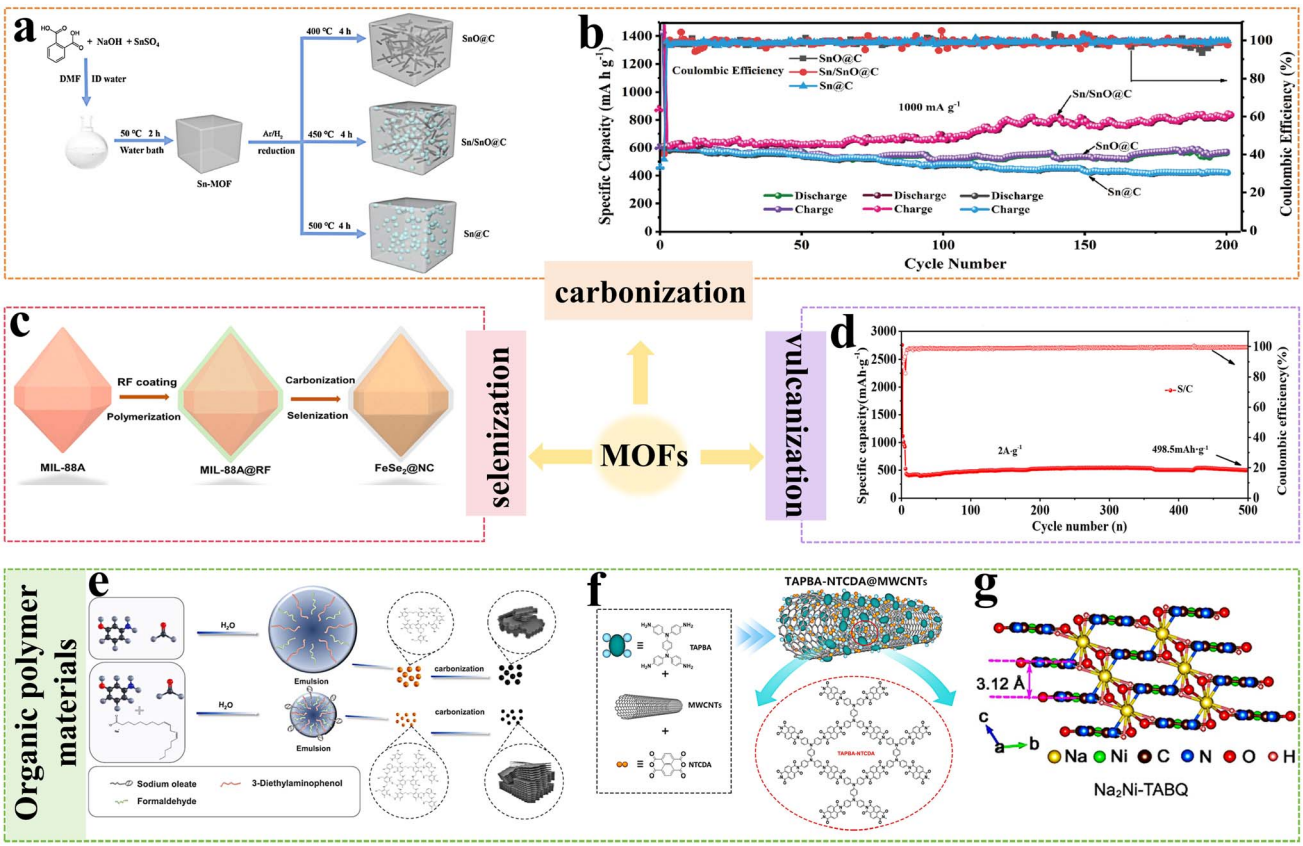

Fig. 5 (a) Schematic illustration of the fabrication of the samples, (b) cycle performance.[49] Reproduced from ref. 49 with permission from Elsevier, copyright 2020. (c) The synthetic process of $FeSe_2$@NC.[50] Reproduced from ref. 50 with permission from Elsevier, copyright 2023. (d) Cycle performance of S/C.[51] Reproduced from ref. 51 with permission from Elsevier, copyright 2024. (e) Schematic diagram of the PFMS preparation process.[52] Reproduced from ref. 52 with permission from Elsevier, copyright 2024. (f) Synthetic process of TAPBA-NTCDA@MWCNTs.[53] Reproduced from ref. 53 with permission from Elsevier, copyright 2023. (g) Crystal structures of Na_2Ni–TABQ.[54] Reproduced from ref. 54 with permission from John Wiley and Sons, copyright 2020.

to adjust their redox and electrochemical performance. In recent years, these materials have shown excellent electrochemical performance as electrode materials for SIBs. However, some small molecule organic compounds will dissolve in the electrolytes, resulting in the shuttle effect of active materials and poor cycling stability. At present, the carbonization of organic polymers to prepare hard carbon (HC) materials, the preparation of composite materials of organic polymers with reduced graphene oxide (rGO) and carbon nanotubes (CNTs), and the fabrication of organometallic polymers can improve the conductivity and stability of organic polymers.

The HC microspheres are obtained by the carbonization of phenol–formaldehyde resin microspheres (PFMS); the graphitization of the materials increases the layer spacing, and facilitates electron and ion transfer (Fig. 5e). The HC microspheres exhibit a high capacity of 96.9 mA h g^{-1} even at a high current density of 5.0 A g^{-1}.[52] As shown in Fig. 5f, the conjugated microporous polyimide (TAPBA-NTCDA) is grown on multi-walled carbon nanotubes (MWCNTs) to form TAPBA-NTCDA@MWCNTs composites.[53] The combination of MWCNTs can enhance the conductivity, increase the active site, and improve the stability of materials. As a cathode material for SIBs, the TAPBA-NTCDA@MWCNTs composites provide a high capacity of 98.4 mA h g^{-1} (0.1 A g^{-1}) and outstanding cycle performance, with a capacity of 51.4 mA h g^{-1} being maintained after over 10 000 cycles (2 A g^{-1}).

The preparation of organometallic polymers can also effectively solve the problems of low conductivity and poor structural stability of organic polymer materials. Ni-coordinated tetramino-benzoquinone (Ni–TABQ) organometallic polymers are synthesized by d–π hybridization.[54] In Fig. 5g, the Ni–N bonds and hydrogen bonds (HBs) in the polymer endow it with a strong two-dimensional (2D) layered structure, which can facilitate electron conduction and Na^+ diffusion. Moreover, the Ni–TABQ shows outstanding rate performance; the discharge capacity is 469.5 mA h g^{-1} at 100 mA g^{-1} and 345.4 mA h g^{-1} at 8 A g^{-1}. Although polymerization is an effective way to prevent the dissolution of organic electrode materials, excessive polymerization will limit the exposure of active sites, thus reducing capacity utilization. Therefore, the control of polymerization to fully release the capacity of materials remains a significant challenge.

2.2. Optimization strategies

In general, since the radius of Na^+ is larger than that of Li^+, the stable active materials with microporous structure need to be selected in ARSIBs, which highlights the significance of selecting electrode materials for achieving high-performance ARSIBs. To obtain the high-performance active materials with appealing stability, further optimization is necessary. Design and optimization strategies, such as morphological engineering, defect engineering, and composite modification, can maximize the performance of active materials. The inherent advantages of materials with optimization strategies can be combined to develop active materials with high energy density and excellent cycling performance, making them very promising candidates for energy storage systems.

2.2.1. Morphology engineering. The morphology of active materials significantly impacts their electrochemical performance, thereby affecting the specific surface area, active sites, and ion migration pathways of materials. One-dimensional (1D) nanostructured materials, characterized by nanowires and nanorods, can provide effective transport pathways for electrons and ions. 2D nanostructured materials, such as nanosheets and nanoflowers, can offer excellent transport pathways for electrons, and reduce the diffusion distances of Na^+. The 3D nanostructured materials mainly include nanomaterials with 3D framework structure and 3D ion transport channels. Due to their unique structure, these materials possess open channels, which significantly increase the abundance of active sites and reduce the diffusion distance of Na^+, thereby improving specific capacity and cycle performance.

As promising 1D nanostructured materials, the special structure of nanowire materials provides abundant active sites for Na^+ storage and transfer. Dense nanowire electrodes possess larger surface areas, offering more effective transfer pathways for Na^+ and electrons, thereby maximizing the application of active materials and enhancing electrochemical performance. For example, the carbon-coated $Na_3V_2(PO_4)_3$ (NVP@C) is fabricated using the electrospinning technique, which is uniformly arranged and densely packed intersecting nanowires (Fig. 6a). In 19 m (mol kg^{-1}) $NaClO_4$–NaOTF electrolyte, the NVP@C cathode provides a wide ESW (3.45 V) and excellent discharge capacity (112.2 mA h g^{-1}), closely approaching its theoretical specific capacity. The NVP//NVP symmetric ARSIBs (Fig. 6b) present excellent energy density (70 W h kg^{-1}) and appealing cycle life, and even after charging/discharging 500 times, the capacity of the batteries can reach 75.6% of their initial capacity, and the CE is 100% (Fig. 6c).[55]

The nanosheet and nano-flower materials are promising 2D nanostructured materials, which provide numerous advantages of increased surface area and affluent Na^+ sites. In Fig. 6d, NVP nano-flowers with large surface area, prepared by high temperature annealing, consist of many ultrathin nanosheets. The symmetric aqueous NVP||$NaClO_4$||NVP micro-batteries exhibit a 2.3 V wide ESW, excellent volume capacity, and outstanding energy density (77 mW h cm^{-3}), surpassing most reported aqueous sodium-ion micro-batteries (Fig. 6e). Notably, even at −40 °C, the CE of this symmetric micro-battery remains as high as 99% (Fig. 6f).[56] As shown in Fig. 6g, the $NaVOPO_4$ materials with various morphologies were fabricated using the hydrothermal approach by adjusting the V/Na ratios in the raw materials. These morphologies encompass microparticles (N6) at a size of 50 μm and ellipsoidal microparticles (N12) at a size of 30 μm × 15 μm, and flower-like micro-sized materials (N24) with 20 μm size.[57] Interestingly, the internally ordered structure of the flower-like N24 provides abundant Na^+ sites, providing buffer space for the volume expansion of the materials throughout the transfer process of Na^+ (Fig. 6h). In Fig. 6i, the discharge capacities of N6 and N12 at 0.2C are 13.7 and 46.8 mA g^{-1}, respectively, while N24 shows the most excellent discharge capacity (67.1 mA h g^{-1}). Furthermore, the capacity

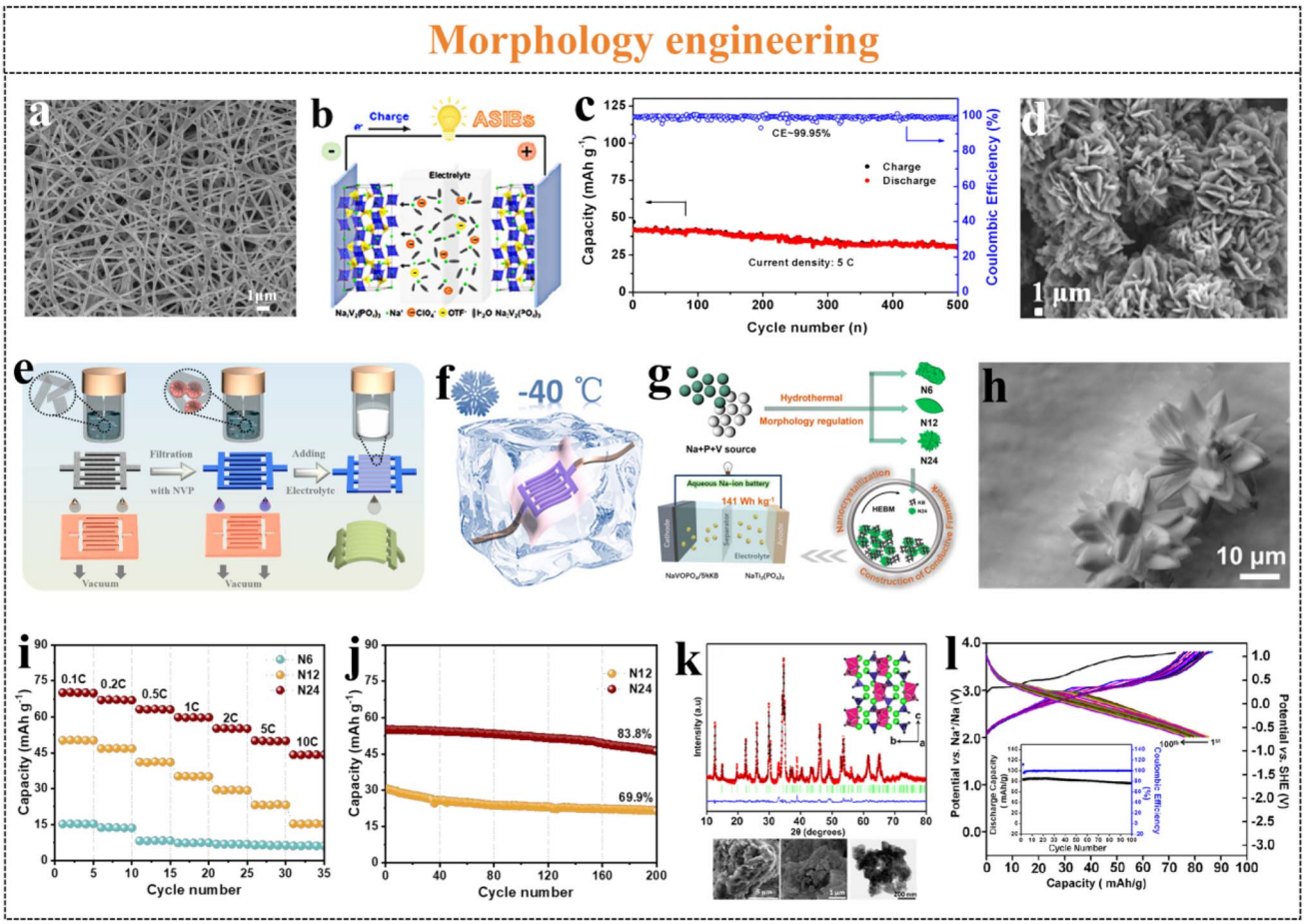

Fig. 6 (a) Morphology of NVP@C nanowires, (b) schematic illustration and (c) cycle performance of the full battery.[55] Reproduced from ref. 55 with permission from John Wiley and Sons, copyright 2021. (d) SEM images of NVP nano-flowers, (e) the symmetric battery NVP||$NaClO_4$||NVP, (f) schematic illustration of the batteries at −40 °C.[56] Reproduced from ref. 56 with permission from Elsevier, copyright 2021. (g) Schematic diagram of the aqueous full-cell, (h) morphological characterization of N24 samples, (i) rate capability and (j) cycle performance of $NaVOPO_4$ materials.[57] Reproduced from ref. 57 with permission from the American Chemical Society, copyright 2022. (k) The structure and (l) cycle performance of Na_2FePO_4F microparticles.[58] Reproduced from ref. 58 with permission from John Wiley and Sons, copyright 2018.

retention of N24 still remains at 83.8% after charging/discharging 200 times (Fig. 6j), demonstrating the phenomenal rate performance and appealing cycle performance. The nano-flower materials composed of ultrathin nanosheets offer a larger specific surface area, while their unique nanostructure shortens the diffusion distance of Na^+, facilitating efficient electron transfer. Consequently, this enables the active materials to engage in electrochemical reactions with optimal efficiency, showing outstanding electrochemical performance.

The 3D framework structure and 3D ion transport channels of the 3D nanostructured materials are crucial in offering more Na^+ sites, which facilitated the insertion/extraction behaviors of Na^+, and enhanced the efficiency of electrochemical reactions. The porous nanomaterials with 3D framework structure offer rapid transfer pathways for Na^+ and electrons, benefiting the diffusion of electrolyte, thereby enhancing interface reaction effects. As shown in Fig. 6k, Na_2FePO_4F microparticles were synthesized using the solvothermal method, exhibiting a morphology characteristic of stacked block-like structures with rough porous surfaces. The porous structure increases the interface contact area and alleviates the material volume expansion during the charging/discharging process. The 3D ion transport channel is beneficial to the insertion/extraction process of Na^+, which further improves its electrochemical activity and cycle stability. In 17 m (mol kg^{-1}) $NaClO_4$ electrolyte, the capacity of Na_2FePO_4F is 84 mA h g^{-1} (1 mA cm^{-2}), and the capacity retention and CE are up to 100% after 100 cycles (Fig. 6l).[58]

The rational design of the nanostructure endows materials with unique surface morphologies, which is conducive to improving the structural stability and obtaining high-performance active materials. The development of multifunctional nanomaterials has made significant contributions to the widespread applications of high-performance ARSIBs in energy storage systems.

2.2.2. Defect engineering. Defect engineering, including intrinsic defects (vacancy defects) and extrinsic defects (heteroatom doping-dominated defects),[59–61] can introduce more active sites to the materials and enhance the structural stability, which is a promising optimizing strategy to obtain

high-performance electrode materials. Introducing defects on the surface or inside the materials to establish additional active sites is crucial, serving as the anchoring points for intermediate species and Na^+, contributing to the insertion/extraction of Na^+. Introducing vacancy defects or doping heteroatoms can alleviate electrostatic repulsion and stress among neighboring layers, aiding in overcoming migration resistance and diffusion hindrance during ion extraction processes. Doping with metal and non-metallic ions can modify the crystal structure, and the materials performance is significantly influenced by the doping locations of ions. Defect engineering provides an effective method to increase active sites and enhance material utilization, effectively improving diffusion kinetics, and thus enhancing the electrochemical performance. The materials can be optimized to enhance electrochemical performance *via* defect engineering strategies, contributing to developments in energy storage applications.

In recent years, tunnel-structured $Na_{0.4}MnO_2$ (NMO) materials have been presented as cathodes with promising electrochemical performance. Subsequently, Ca^{2+} was doped to develop a novel cathode material, $Ca_{0.07}Na_{0.26}MnO_2$ (CNMO), for ARSIBs,[62] and CNMO showed enhanced discharge capacity and appealing cycle performance compared to NMO. As shown in Fig. 7a, the doped Ca^{2+} at the Na(1) sites can reduce the manganese ions at the adjacent manganese sites, and the doped Ca^{2+} at the Na(2) and Na(3) sites in the manganese oxide skeleton can form vacancy defects, thus improving the diffusion kinetics of Na^+. The CNMO displays higher capacity enhancement compared with NMO, and the capacity of CNMO increased 43% at 50C. In addition, active carbon//CNMO (AC//CNMO) full batteries deliver phenomenal rate performance and superior cycle performance, and the capacity retention can reach 98.8% even after charging/discharging 1000 times at 50C (Fig. 7b). The above suggest that the doping of Ca^{2+} leads to vacancy defects, increasing active sites and facilitating the transfer process of Na^+, which improves the electrochemical performance.

NVP has the advantages of high operating voltage, 3D framework structure, and appealing stability, making it a potential cathode material for ARSIBs.[63–66] However, there are challenges in improving the rate performance and cycling stability, which need to be solved for wide application compatibility. Introducing transition metal ions (Cr^{3+}, Ti^{3+}, Mg^{2+}, Zr^{3+}),[67–70] nonmetallic ions such as F^- (ref. 71) and rare earths ions (Gd^{3+} and Y^{3+})[72,73] into NVP materials can increase defect sites, leading to enhanced capacity, appealing cycle performance, and excellent energy density. The doping of F^- can not only introduce extrinsic defects, but also significantly increase the working voltage, further enhancing structural stability, because of its strong inductive effect and high electronegativity. $Na_3V_2(PO_4)_2F_3$ (NVPF) presents outstanding reversible theoretical capacity (128 mA h g^{-1}) and a wide ESW (3.8 V), making it a suitable cathode. As shown in Fig. 7c, the crystal structure of NVPF is made up of $[V_2O_8F_3]$ octahedra and $[PO_4]$ tetrahedra, where two $[V_2O_8F_3]$ octahedra are connected by a F along the *c*-axis. Stable phosphate–metal bonds can develop on cathodes in fluorophosphate and phosphate materials, lowering the possibility of oxygen release.[74] Due to the existence of PO_4^{3-} polyanions, the material volume expansion can be considerably reduced throughout the charging/discharging process of Na^+.

The $Na_3V_{1.9}Y_{0.1}(PO_4)_3F_3$/C (NVYPF/C) materials are prepared by adding an appropriate amount of rare earth element yttrium (Y) to NVPF, where some V sites are replaced by Y, which can increase the active sites and enhance the performance of the materials (Fig. 7d). The V^{3+} sites are replaced by Y^{3+} with a larger radius in the NVPF structure, leading to vacancy defects, achieving rapid Na^+ transfer, and both Y–O and V–O bonds can improve the conductivity and stability of materials. Furthermore, the inert Y^{3+} substitutes the V^{3+} sites in the NVPF, which can buffer material volume expansion throughout the transfer process of Na^+, thus potentially improving the structural stability. As shown in Fig. 7e, NVYPF/C exhibits excellent discharge capacity (121.3 mA h g^{-1}) and appealing cycle performance, and the capacity still remains at 93.5% of the initial capacity after charging/discharging 200 times.[73]

The organic ligand CN_6^- in $NaCu[Fe(CN)_6]$ (NaCuHCF) is replaced by other organic ligands, which change the framework structure of PBAs and form internal vacancies, thereby enhancing the cycle performance of materials. The capacity retentions of $Na_xCu[Fe(CN)_5(C_6H_4N_2)]$ (Na_xCuCNPFe) and $Na_xCu[Fe(CN)_5(CH_3C_6H_4NH_2)]$ (Na_xCuTolFe) cathodes are all 50% in 1 M Na_2SO_4 electrolytes, far higher than that of NaCuHCF (0%) after charging/discharging 2000 times (Fig. 7f).[75] These results demonstrate that ligand substitution strategies can effectively optimize the internal structure of materials to enhance structural stability, and increase the active sites for the transfer of Na^+. Simultaneously, both doping and substitution methods give rise to additional ions or ligands occupying a small amount of sodium sites. Excessive occupancy would have a counterproductive effect, leading to reduced capacity and decreased cycling performance.

2.2.3. Composite modification. Composite materials are prepared by combining two or more active materials, which can endow the materials with high energy density and appealing stability. According to numerous studies, compared to a single electrode material, the composite materials can leverage the strengths of multiple materials and exhibit appealing electrochemical performance.[76] The combination of different materials increases the surface area and provides abundant attachment sites for Na^+ transfer. Meanwhile, it can decrease the volume expansion of active materials, promote conductivity, and enhance the structural stability throughout the charging/discharging process.

The porous structure and excellent conductivity of carbon materials play a crucial role in shortening ion transport pathways, reducing the interface resistance and polarization, and making insertion/extraction of Na^+ convenient. As a substrate or surface coating of active materials, the addition of carbon materials is conducive to prevent material aggregation, ensuring better contact between materials and electrolytes. The commonly used carbon materials are carbon nanofibers (CNFs), CNTs, and rGO. CNTs with unique tubular structure exhibit great conductivity, expansive surface area, and appealing

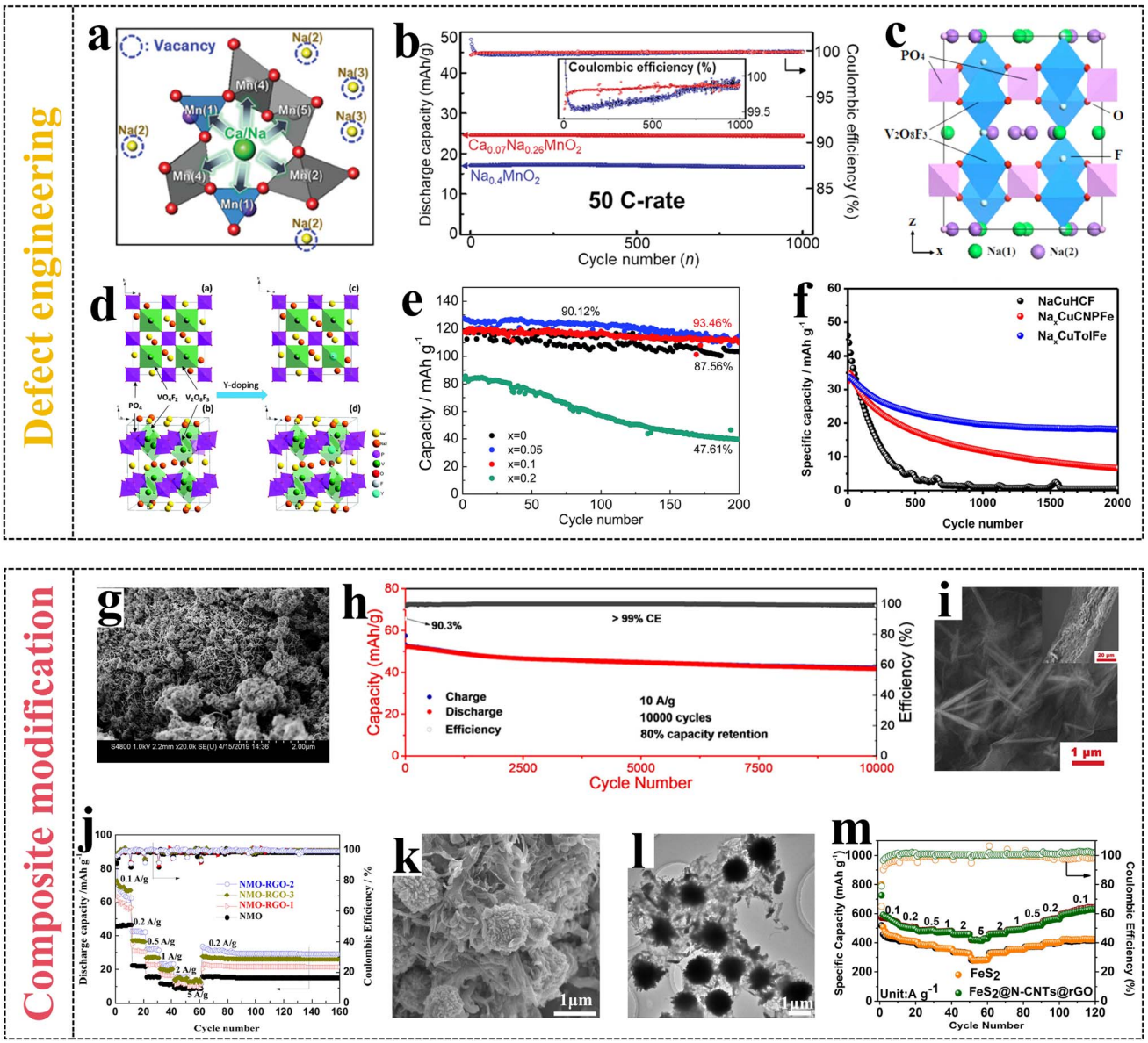

Fig. 7 (a) CNMO with local structure around Na(1), (b) cycle performance of CNMO.[62] Reproduced from ref. 62 with permission from John Wiley and Sons, copyright 2020. (c) Crystal structure of NVPF.[74] Reproduced from ref. 74 with permission from the American Chemical Society, copyright 2014. (d) Schematic illustration of the NVPF crystal structure before and after Y-doping, (e) cycle performance of NVYPF/C.[73] (f) Capacity retention of NaCuHCF, $Na_xCuCNPFe$ and $Na_xCuTolFe$.[75] Reproduced from ref. 75 with permission from Elsevier, copyright 2022. (g) SEM image of NiHCF@CNTs, (h) cycle performance.[77] Reproduced from ref. 77 with permission from the American Chemical Society, copyright 2020. (i) Morphology of NM/rGO, (j) cycle performance.[78] Reproduced from ref. 78 with permission from Elsevier, copyright 2018. (k) SEM images and (l) TEM images of the FeS_2@NCNTs@rGO, (m) rate capability.[79] Reproduced from ref. 79 with permission from Elsevier, copyright 2021.

mechanical performance. Nevertheless, using CNTs alone as electrode materials for SIBs makes it difficult to meet practical applications. Therefore, combining CNTs with other active materials is indispensable to enhancing electrochemical performance. Nickel hexacyanoferrate with CNT (NiHCF@CNTs) nano-materials are synthesized using a typical coprecipitation method.[77] In Fig. 7g, CNTs are intertwined with NiHCF nanoparticles to form a 3D interconnection network, which helps to enhance the interaction kinetics and conductivity of electrode materials. After 10 000 cycles, the NiHCF@CNTs cathode shows high energy density and appealing cycle performance, and capacity retention is still at 80% at 10 A g^{-1} (Fig. 7h).

The composite material $Na_4Mn_9O_{18}$/reduced graphene oxide (NM/rGO) exhibits enhanced electrochemical performance, because of the excellent in-plane conductivity, extensive surface area, and high mechanical durability of graphene.[78] Having NM/rGO films without current collectors, conductive additives and binders as the cathodes of ARSIBs streamlines the synthesis process and reduces the cost of the battery. As shown in Fig. 7i, the needle-like NM is densely fixed onto the wrinkled graphene sheet to form the NM/rGO composite material with 3D

channels, which provides a fast electron conduction path, enhances the structural stability, and reduces mechanical stress caused by the transfer of Na^+. As shown in Fig. 7j, the NM/rGO offers great rate performance and appealing cycle performance, and its specific capacity is about 83 mA h g^{-1}, marking an approximately 78% increase compared to NM.

FeS_2 was combined with N-doped CNTs (NCNTs) and rGO using the hydrothermal method to prepare FeS_2@NCNTs@rGO composites with microsphere structure.[79] The urchin-like FeS_2 and conductive NCNTs within the layered rGO form a stable network structure (Fig. 7k and l), which helps alleviate the stress and strain caused by Na^+ transfer. The unique structure of FeS_2@NCNTs@rGO enables effective electron charge transfer and reduces the transfer pathway of Na^+, significantly enhancing the conductivity and structural stability of the composite materials. The incorporation of NCNTs and rGO enlarges the specific surface area, buffers the volume expansion of composite materials throughout the cycling process and reduces the dissolution of the electrode materials caused by related strains, thereby leading to outstanding electrochemical performance. As shown in Fig. 7m, compared with FeS_2, the FeS_2@NCNTs@rGO composite materials exhibit excellent specific capacity, phenomenal rate capability, and appealing cycle performance, after charging/discharging 750 times at 2 A g^{-1}. In the FeS_2@NCNTs@rGO composite materials, the bent NCNTs form a cross-linked network structure, and FeS_2 is wrapped together with NCNTs and rGO to form a 3D structure, which provides an additional electron pathway, accelerates the transfer of Na^+, and effectively enhances the performance of active materials, thereby facilitating the attainment of high-performance SIBs.

Overall, the composite of two or more materials can synergize their respective advantages, significantly enhancing the conductivity and designing active materials with excellent energy density and phenomenal cycle performance. Nevertheless, the bonding mechanisms between multiple materials (physical or chemical bonding) require further investigation.

3. Anode materials

In recent years, many studies have shown that carbon materials, polysulfides, and poly-anionic compounds are the common anode materials for ARSIBs.[80] Compared with the cathodes, the anodes with low potential and poor stability need extensive attention, and the further development of anodes is significant for enhancing the electrochemical performance of ARSIBs. The battery construction and reaction mechanism of SIBs are analogical to those of LIBs, and Li can serve as the anodes for LIBs, but Na is unsuitable for SIBs. The reasons are as follows: (1) Na with a low melting point (97.7 °C) presents safety issues, (2) Na exhibits strong chemical reactivity with water-based electrolytes, (3) Na will form dendrites during the charging and discharging process, causing short circuits. It is an effective strategy to use non-metal anodes instead of Na anodes in ARSIBs, but the use of non-metal anodes will result in a decrease in energy density. According to previous reports, high-performance sodium-rich active materials, "water-in-salt" (WIS) electrolytes and the sodium compensation method can replenish the Na^+ lost during the charging/discharging processes, effectively improving the energy density.[81–83] In ARSIBs, Na undergoes intense reactions with the aqueous electrolyte, and there are problems of dissolution and structural collapse of some active materials in the aqueous electrolyte, hindering the development of anode materials. Therefore, it is essential to optimize active materials for enhancing the performance of ARSIBs.

3.1. Carbon materials

Based on differences in microstructure and the degree of graphitization, carbon-based electrode materials can be classified as graphite, soft carbon, or HC. Compared with Li^+, Na^+ with a larger radius and mass are difficult to be quickly inserted/extracted in graphite electrodes.[84,85] Both HC (such as biochar, metal organic framework-based carbon, and other porous AC materials) and soft carbon (such as CNTs) have been effectively used as anode materials for SIBs.[86–89] HC is formed by highly disordered stacking of graphite-like crystallites and graphene-like sheets, and there is a strong force between the carbon layers, giving it a tight layered structure. HC has advantages of porous structure and high conductivity, which provide excellent performance. Nevertheless, the problems of low CE and poor cycling stability need to be resolved in the practical applications of carbon materials for ARSIBs.

In ARSIBs, carbon materials are mainly used as substrates to composite with other active materials as anode materials, which can enhance the conductivity and increase Na^+ active sites. As shown in Fig. 8a, the MWCNT is used as the core to fabricate MWCNT@polyimide core–shell nanowires with a polypyrrole coating (MWCNT@polyimide/polypyrrole) as the anode of ARSIBs.[90] The existence of MWCNT would be beneficial for accelerating the Na^+ transfer speed throughout the charging/discharging process, and making up for the seriously poor conductivity of polyimide. Moreover, the polypyrrole improves the conductivity of the material, prevents degradation of electrode material structure, and improves the cycling stability of the materials. After 100 charging/discharging cycles, the MWCNT@polyimide/polypyrrole nanowire presents a capacity retention of 77.8%, and the electrode material without expansion and structural damage shows appealing electrochemical performance (Fig. 8b).

3.2. Polysulfides

Polysulfides are at risk of dissolving in aqueous electrolytes, ultimately causing irrecoverable H_2S gas, irreversible material structure damage and high interfacial resistance, eventually resulting in short cycle life of the battery. As the dissolution occurs at the electrode–electrolyte interface, the energy density and cycling stability of the batteries principally rely on the characteristics of electrolytes and active materials. Carbon materials with stable structure provide large surface area and abundant anchoring sites, making them suitable hosts for sulfides and effectively alleviating the issues of polysulfide dissolution. Tubular mesoporous nitrogen-doped carbon

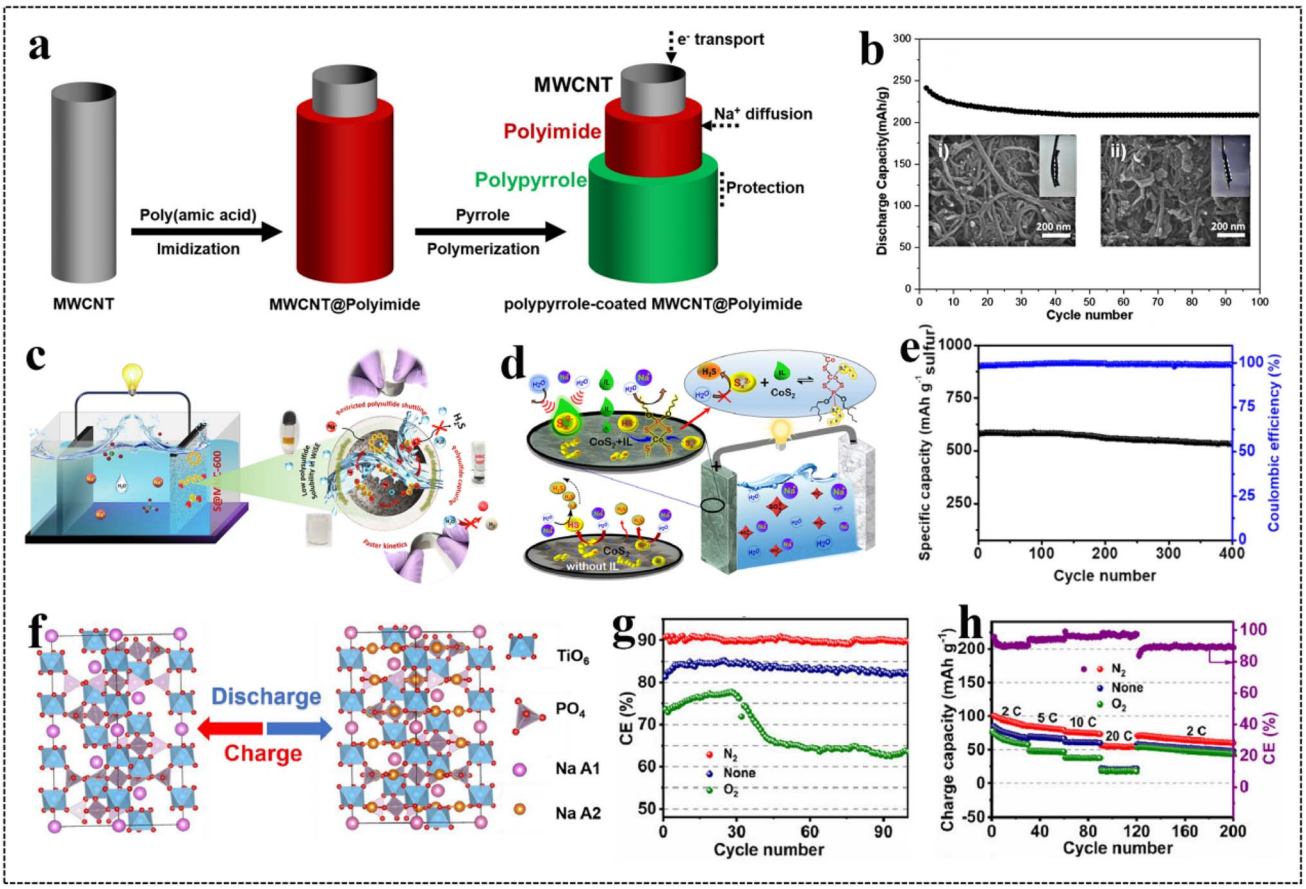

Fig. 8 (a) The synthetic process of MWCNT@polyimide/polypyrrole, (b) cycle performance.[90] Reproduced from ref. 90 with permission from Elsevier, copyright 2021. (c) Aqueous Na/S battery S@C//$Na_{0.44}MnO_2$.[22] Reproduced from ref. 22 with permission from Elsevier, copyright 2022. (d) Schematic representation of the S@Co-IL//$Na_{0.44}MnO_2$ full battery, (e) cycle performance.[91] Reproduced from ref. 91 with permission from Elsevier, copyright 2022. (f) Na^+ storage mechanism, (g) rate capability, and (h) cycle performance of NTP@C.[98] Reproduced from ref. 98 with permission from Elsevier, copyright 2023.

(MNC-600) materials exhibit high surface area and great conductivity, providing abundant anchoring sites and improving the redox kinetics. Sulfur is embedded in the MNC-600 to prepare S@MNC-600 (S@C) as the anode of ARSIBs (Fig. 8c). As a suitable host for S, NMC-600 improves the conductivity and structural stability of the S@C materials. S@C still maintains 78.2% of the initial capacity, and the CE is about 98.2% after charging/discharging 300 times. The high-performance ARSIBs are assembled with the S@C anode, $Na_{0.44}MnO_2$ cathode and 17 m $NaClO_4$ electrolyte, and the energy density of S@C//$Na_{0.44}MnO_2$ can reach 110.6 W h kg^{-1}.[22]

Fig. 8d shows that 70% elemental sulfur, CoS_2, and 1-butyl-3-methylimidazolium-*o*,*o*-bis(2-ethylhexyl)dithiophosphate ionic liquid (BMIm-DDTP-IL) are present in the anode (S@Co-IL) for aqueous rechargeable Na/S batteries.[91] After charging/discharging 100 times, the S@Co-IL anode shows appealing cycle performance, and the capacity retention and CE remain at 98% and 100%, respectively. Moreover, the synergistic effect of BMIm-DDTP-IL and CoS_2 can enhance conductivity and efficiently inhibit the structural collapse of polysulfides. As shown in Fig. 8e, the S@Co-IL//$Na_{0.44}MnO_2$ full battery exhibits outstanding discharge capacity of 778 mA h g^{-1} (based on the mass of S) at 1C and excellent cycle performance, with 91.8% retention of its initial capacity, and the CE is 100% after charging/discharging 400 times at 2C.

3.3. Polyanionic compounds

NASICON-type polyanionic compounds have garnered widespread attention owing to their high structural stability, large ion channels, and abundant active sites.[92–95] Among them, $NaTi_2(PO_4)_3$ (NTP), $Na_3Fe_2(PO_4)_3$ (NFP), $Na_3MnTi(PO_4)_3$ (NMTP), and $Na_2VTi(PO_4)_3$ (NVTP) Na-rich polyanion compounds are regarded as the most promising anode materials for high-performance ARSIBs, due to their structural advantages.

3.3.1. $NaTi_2(PO_4)_3$. NASICON-type NTP with 3D framework structure composed of TiO_6 octahedra and PO_4 tetrahedra is a promising anode material for ARSIBs. The structural advantages of NTP can provide sufficient space for rapid transfer of Na^+ and alleviate the volume change during the charging/discharging process.[96,97] Although NTP is a common anode material for ARSIBs, it still faces the challenges of low CE and significant capacity decay. Improved methods, such as carbon

coating, heteroatom doping, and preparing composite materials, can effectively solve this problem.

The conductivity of materials can be enhanced and the electron transport path can be shortened by applying a carbon layer to the surface of NTP. The conductive carbon layers on the materials increase the Na^+ attachment sites, facilitating insertion/extraction behaviors of Na^+, and alleviating volume expansion throughout the charging/discharging process. The porous NTP micron materials coated with a nano-carbon layer (NTP@C) exhibit a unique single crystal structure, which promotes rapid transport of electrons and Na^+ (Fig. 8f).[98] Furthermore, the carbon layer enhances the conductivity of NTP and serves as a protective interface, shields the electrode material from dissolution, and enhances its stability. In three electrolytes (1 M Na_2SO_4 electrolyte, 1 M N_2-purged Na_2SO_4 electrolyte, and 1 M O_2-dissolved Na_2SO_4 electrolyte), the NTP@C anodes provide both excellent capacity and phenomenal CE (none: 87.3 mA h g^{-1}, 81.4%; N_2: 101.4 mA h g^{-1}, 90.8%; O_2: 79.2 mA h g^{-1}, 73.6%) (Fig. 8g and h). It is well known that precious metals show excellent conductivity, and the carbon layer containing precious metals can also provide enhanced conductivity. The NTP@C/Ag materials are prepared as the anode materials for ARSIBs by adding Ag to the NTP carbon layers.[99] Compared with NTP materials, NTP@C/Ag materials obviously show higher conductivity, better structural stability and more excellent electrochemical performance. Even after charging/discharging 400 times at 5C, the capacity retention of materials capacity is still at 82.7% (Fig. 9a). Therefore, coating a carbon layer on the active materials is an effective method to improve the conductivity and enhance the structural stability of materials.

As is well known, the hydrogen evolution potential is −0.817 V (*vs.* Ag/AgCl). However, as the anode of ARSIBs, the Ti^{4+}/Ti^{3+} redox potential in NTP is −0.807 V (*vs.* Ag/AgCl), and it faces a great risk of HER in aqueous electrolytes, which hinders the wide applications of NTP anodes in ARSIBs, so it is necessary to find an effective improvement strategy. Heteroatom doping can solve this problem, which can introduce vacancy defects to establish additional sodium storage sites, alleviate the electrostatic repulsion and stress among layers, help to overcome the migration resistance and diffusion obstacles. $Na_{1.5}Ti_{1.5}Fe_{0.5}(PO_4)_3$ (NTFP) was prepared by doping Fe^{3+} into NTP, in which the combination of Fe^{3+}/Fe^{2+} and Ti^{3+}/Ti^{4+} redox pairs increased the working potential to −0.721 V, availably preventing overlap with the potential of water decomposition (Fig. 9b).[100] The different bond lengths of Fe–O and Ti–O result in different bond angles of Ti–O–P and Fe–O–P, changing the symmetry of the O–P–O bonds and decreasing the average distance between O–P–O, resulting in a slight asymmetric feature in NTFP, according to the pair distribution function (PDF) analysis (Fig. 9c and d). Moreover, the NTFP anode presents high discharge capacity (122.1 mA h g^{-1}), and appealing rate performance in 5 M $NaClO_4$ electrolyte. Subsequently, $Na_{1+x}Al_xTi_{2-x}(PO_4)_3$/C ($x$ = 0, 0.05, 0.10, 0.20) were prepared by doping Al^{3+} on NTP, which establishes vacancy defects and introduces extra active sites.[101] Although the doping of Al^{3+} has no evident impact on the structure of the materials, it accelerates the migration of Na^+, improves reaction kinetics, and enhances the electrochemical performance. Heteroatom doping can introduce defects for active materials, increase the active sites of Na^+, and enhance the structural stability, making it a promising anode for ARSIBs.

Combining two or more electrode materials to prepare composite materials can leverage the strengths of each material and enhance the electrochemical performance. The MWCNT with pore structure possess enhanced conductivity, high specific surface area, and appealing mechanical performance. As anode materials for ARSIBs, NTP-MWCNT composite materials are beneficial for enhancing conductivity, increasing specific surface area, and facilitating the transfer process of Na^+, thereby improving the electrochemical performance of the composite materials (Fig. 9e).[102] In Fig. 9f, the NVPF-SWCNT//NTP-MWCNT full batteries exhibit a discharge capacity of 75.2 mA h g^{-1}, a high CE (99%), and an excellent energy density (150 W h kg^{-1}). In addition, MXene presents excellent mechanical performance and high conductivity, and the existence of O, OH, and F enables MXene to form HBs with other active materials. As shown in Fig. 9g and h, the combination of NTP nanoparticles and MXenes forms the composite materials NTP/MXenes,[103] where the introduction of external particles between MXene sheets effectively prevents material accumulation. As shown in Fig. 9i, the NTP/MXene composites deliver outstanding cycle performance and excellent capacity retention (88%) even after charging/discharging 1500 times (20C). The fabrication of composite materials can combine the advantages of various materials, enhance the structural stability, and increase the Na^+ active sites, which enables the composite materials to provide high energy density and excellent cycle performance.

3.3.2. $Na_3MnTi(PO_4)_3$ and $Na_2VTi(PO_4)_3$. In recent years, NISICON-structured NMTP and NVTP have displayed high energy density and appealing structural stability. NMTP with a 3D framework structure is made up of MnO_6/TiO_6 octahedra and PO_4 tetrahedra, which exhibit sufficient Na^+ storage capacity and reversible redox activity.[104,105] NMTP is a potential active material in the construction of symmetric batteries, and can be utilized as both the anode and cathode of ARSIBs due to Mn^{3+}/Mn^{2+} and Ti^{4+}/Ti^{3+} redox couples.[106,107] As shown in Fig. 10a, NMTP serves as an electrode material for symmetric ARSIBs, Na^+ is extracted or inserted from NMTP to form $Na_2MnTi(PO_4)_3$ and $Na_4MnTi(PO_4)_3$ intermediates during the charging/discharging process, and the redox potential is not in the range of HER/OER, due to the existence of Mn^{3+}/Mn^{2+} and Ti^{4+}/Ti^{3+} redox couples. Furthermore, the symmetrical battery (NMTP//NMTP) presents high reversible capacity (56.5 mA h g^{-1}) and outstanding cycle performance, with a phenomenal capacity retention of 98% and high CE of 99% after 100 cycles (Fig. 10b and c).[108] The NMTP materials demonstrate excellent electrochemical performance, offering new opportunities for the fabrication of high-performance ARSIBs.

The NISICON-structured NVTP consists of VO_6/TiO_6 octahedra and PO_4 tetrahedra to form a 3D framework. As shown in Fig. 10d, during the charging/discharging process, Na^+ was extracted from NVTP to form $NaVTi(PO_4)_3$ intermediates through the V^{4+}/V^{3+} redox couple, while Na^+ transfers to another electrode

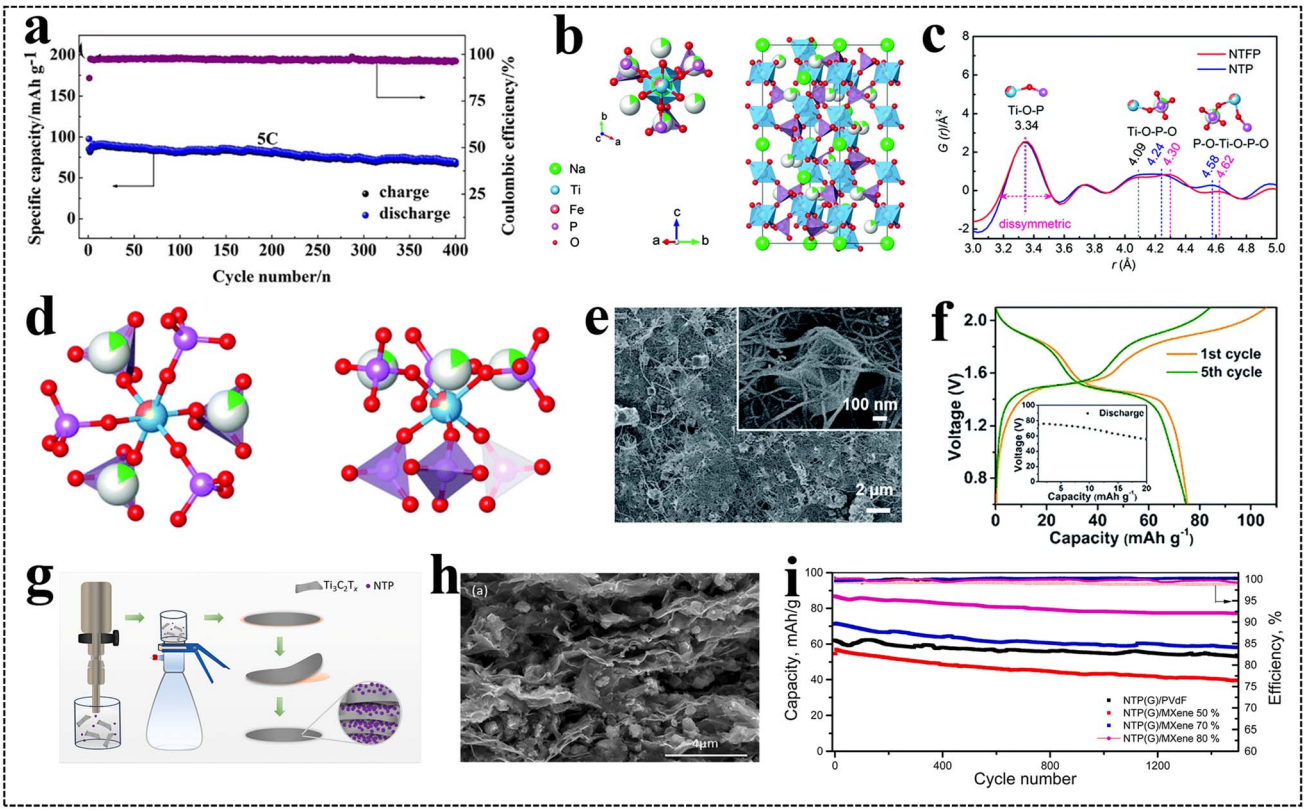

Fig. 9 (a) Cycle performance of NTP@C/Ag.[99] Reproduced from ref. 99 with permission from Elsevier, copyright 2018. (b) Schematic illustration of the crystal structure of NTFP, (c) representative PDF data of NTFP. (d) Ti/Fe-centered local structures of NTFP.[100] (e) SEM images of NTP-MWCNT, (f) cycle performance of the NVPF-SWCNT//NTP-MWCNT full battery.[102] (g) Preparation procedure, (h) SEM images, and (i) long-term cycling performance of NTP/MXene.[103] Reproduced from ref. 103 with permission from Elsevier, copyright 2021.

to form $Na_4VTi(PO_4)_3$ with the redox reactions with the Ti^{4+}/Ti^{3+} redox couple. In addition, the symmetric ARSIBs exhibit excellent rate performance, high energy density of 55.9 W h kg^{-1}, and appealing cycle performance (Fig. 10e). After charging/discharging 1000 times at 5 A g^{-1}, the capacity retention of this battery is still at 60%, and the CE is closed to 100%.[95]

3.3.3. $Na_3Fe_2(PO_4)_3$. The NISICON-structured NFP features a 3D framework with interconnected channels formed by the sharing of angles between the FeO_6 octahedra and PO_4 tetrahedra, which facilitates the diffusion and storage of Na^+ (Fig. 10f). Moreover, the NFP serves as an anode for ARSIBs delivering high CE (90.8%) and outstanding rate performance, and the capacity can return to the initial capacity, when the current density is brought from 100C back to 2C.[109] As shown in Fig. 10g, the ARSIBs are fabricated by using $Na_2Mn[Fe(CN)_6]$, NFP, and 17 m $NaClO_4$ electrolyte. During the charging process, Fe^{2+} in the $Na_2Mn[Fe(CN)_6]$ is oxidized to Fe^{3+} along with the transfer of Na^+ from the cathode to anode, while Fe^{3+} in NFP is reduced to Fe^{2+}, and the discharging process is opposite to the charging process. After 700 cycles at 5C, the NFP//$Na_2Mn[Fe(CN)_6]$ battery shows 75% discharge capacity of its initial capacity and the CE is 100%, demonstrating outstanding cycle performance and high stability (Fig. 10h).

Currently, carbon materials, polysulfides, and polyanionic compounds are the most common anode materials for ARSIBs. Optimization strategies for these materials include carbon coating, heteroatom doping, and preparation of composite materials to alleviate material volume expansion, reduce charge diffusion distance, and increase conductivity, which can provide excellent cycling stability and rapid kinetics.

4. Recent development of electrolytes

The electrolyte is an important component of the battery, which is the intermediary for ion transfer between the anode and cathode and has a significant impact on the electrochemical performance of the battery. Outstanding electrolytes should possess excellent stability, superior conductivity, and a wide ESW. Different from traditional organic electrolytes, aqueous electrolytes exhibit high conductivity, safety, and eco-friendliness. Aqueous electrolytes can be divided into liquid electrolytes and hydrogel electrolytes according to the physical properties of the electrolyte; an aqueous electrolyte solution is often influenced by the inherent properties of electrolyte components (salts concentrations, solubility, and freezing point).

4.1. Solvation behavior in electrolytes

The solvation behavior determines the composition, thickness, and structure of the solid electrolyte interphase (SEI), which

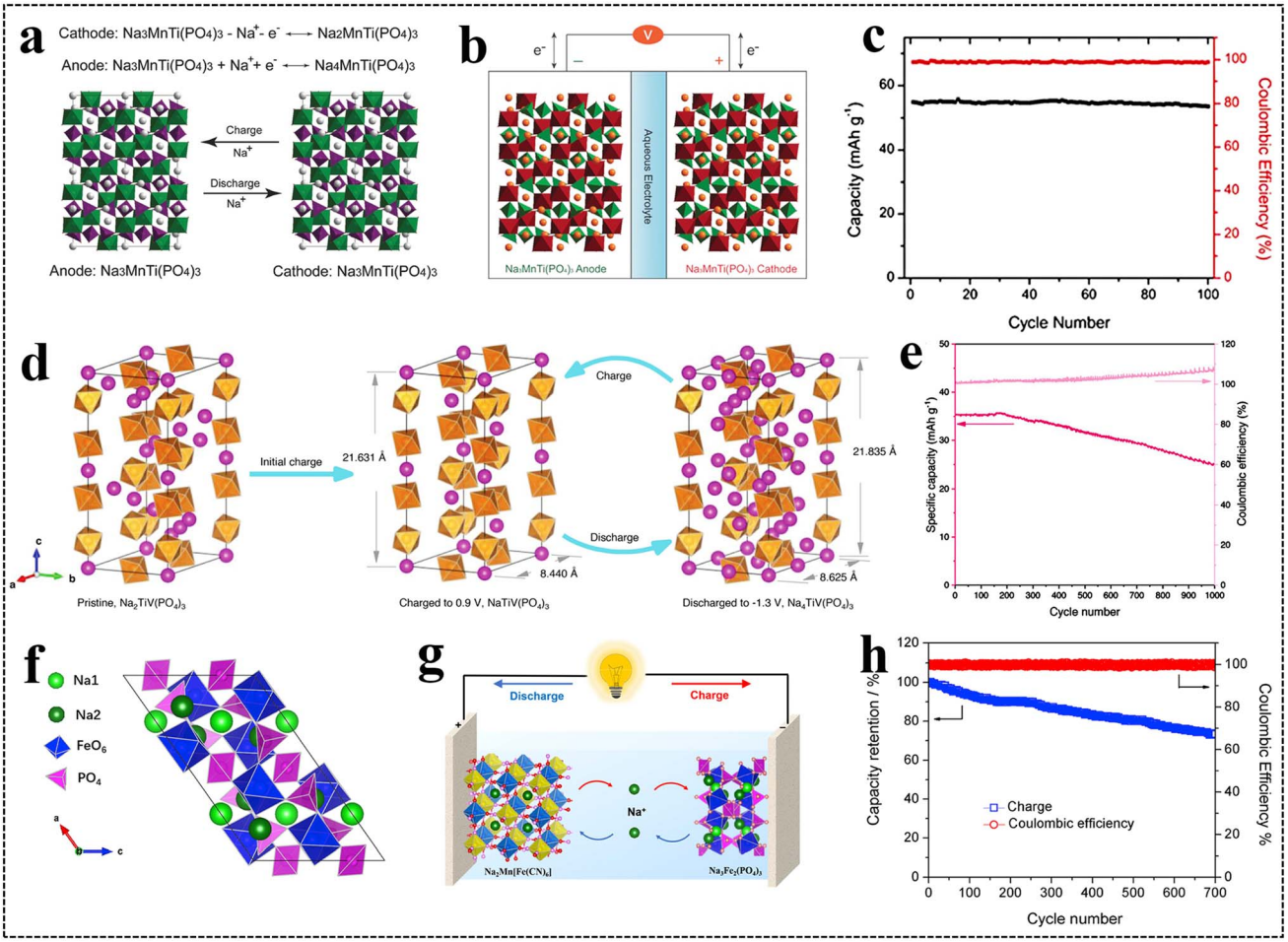

Fig. 10 (a) Mechanism diagram and (b) schematic illustration of the symmetric ARSIBs, (c) cycle performance.[108] Reproduced from ref. 108 with permission from John Wiley and Sons, copyright 2016. (d) Charge/discharge reaction mechanism of NVTP, (e) cycle performance of the symmetrical ARSIBs.[95] Reproduced from ref. 95 with permission from John Wiley and Sons, copyright 2024. (f) The crystal structure of the NFP anode, (g) schematic illustration of ARSIBs, (h) cycle performance at 5C.[109] Reproduced from ref. 109 with permission from Elsevier, copyright 2019.

indirectly affects the electrochemical performance of batteries. The solvation structure refers to a relatively stable sheath structure formed by the interactions among the cations, anions, solvent molecules and additives molecules. It has been reported that solvated ions typically possess two solvation layers, a tight first solvation layer and a relatively incompact second solvation layer.[110] The strong electrostatic forces and coordination bonds between solvent molecules and cations lead to a balance of attraction and repulsion, forming the tight first solvation layer. The second solvation layer is slightly incompact, including solvent molecules influenced by remote dipole interactions, solvent molecules attracted by the cation, free solvent molecules, and free anions.[111–113] During the charging/discharging process, cations undergo an insertion/extraction process within the active materials. Before cations can be inserted into the electrode materials through the SEI layer, desolvation should occur, including the removal of solvent molecules and anions. The desolvation process of cations significantly affects the discharge capacity, ESW, CE, and cycle performance of batteries.

As an excellent solvent, water molecules exhibit high polarity and a high dielectric constant, where the lone pairs on the oxygen atom can coordinate with cations, which increases the oxidation potential of the water, thus improving the stability. These characteristics grant water molecules a strong solvation capability for most salts. There are many more water molecules than salt in a diluted sodium salt solution with a concentration of less than 5 M, which usually results in two solvation layers surrounding the Na^+. When the salt concentration exceeds 9 M, there are hardly sufficient water molecules to generate the first solvation layer, and the WIS electrolytes can be regarded as dissolved salt. For example, the 9.26 m NaOTF electrolyte can expand the ESW to 2.5 V in ARSIBs.[114] The concentrated NaOTF electrolyte prevents the formation of the first solvation layer around Na^+, and only an incompact second solvation layer is formed, which facilitates the desolvation behavior of Na^+ throughout the charging/discharging process. The concentrated electrolyte (9.26 m NaOTF) contains much more salt than free water, which effectively inhibits the HER/OER. As for 17 m $NaClO_4$ + 2 m NaOTF electrolyte (19 m electrolyte), the solvation

structure of Na^+ is formed of the ClO_4^-, OTF^-, and water molecules, and an SEI composed of NaF, Na_2O, and NaOH is formed on the anode.[55] The NVP//NVP symmetric batteries with the 19 m electrolyte present a wide ESW of 1.75 V, excellent energy density (70 W h kg^{-1}), and outstanding electrochemical performance.

4.2. Liquid electrolyte

4.2.1. Diluted electrolytes. In diluted electrolytes, there is a substantial amount of free water, resulting in the formation of two solvation layers around Na^+, and one Na^+ coordinated with six water molecules in the solvation layers. The diluted electrolytes include 1 M Na_2SO_4,[115,116] 1 M $NaNO_3$,[117,118] 1 M CH_3COONa,[119,120] and 1 M NaCl,[121,122] which show high conductivity, are of low cost, and have great potential in ARSIBs. Among them, 1 M Na_2SO_4 can be compatible with various electrode materials such as $Na_{0.44}MnO_2$,[123] $NaFePO_4$,[124] NTP,[125] and $Na_2Ni[Fe(CN)_6]$.[126] As shown in Fig. 11a, the Na^+ insertion/extraction processes of $Na_2FeM_5(CN)_6 \rightarrow NaFeM_5(CN)_6 \rightarrow Na_2FeM_5(CN)_6$ indicate that only 50% Na^+ can freely insert/extract for electrochemical reactions. Furthermore, the $NaTi_2(PO_4)_3$@C// $Na_2(MnCoNiCuZn)_{0.2}[Fe(CN)_6]$ (NTPC//M5HCF) battery with 1 M Na_2SO_4 electrolyte shows appealing rate performance and excellent cycling stability. In high-conductivity dilute electrolyte solution, the battery demonstrates appealing cycle performance, and the battery capacity still remains at 87% after charging/discharging 1000 times at 1C high current density (Fig. 11b).[116] In 1 M $NaNO_3$ electrolyte, the Bi_2Se_3 anode possesses a phenomenal discharge capacity of 90 mA h g^{-1},[118] because of the formation of an SEI (Na_2O, NaOH, and Na_2CO_3) around the anode.

The electrochemical performance of ARSIBs can be effectively enhanced by mixing two or more diluted electrolytes to prepare hybrid-ion electrolytes. Among them, aqueous Na/Mg, Na/Li, and Na/Zn hybrid ion batteries collectively show phenomenal electrochemical performance.[127–130] An aqueous Na/Mg hybrid ion battery is assembled with 1,4,5,8-naphthalenetetracarboxylic anhydride anthraquinone (PNTAQ) polymer material, MnO_2, and 1 M $MgCl_2$ + 0.5 M NaCl hybrid electrolyte. During the charging/discharging process, the insertion/extraction of Na^+ and Mg^{2+} occurs in the active material (Fig. 11c), thereby improving the discharge capacity and cycle performance of the battery, and the capacity of the PNTAQ//MnO_2 battery is only reduced by 12.8% (1000 mA g^{-1}) after 1000 cycles (Fig. 11d).[127] $Zn(CH_3COO)_2$ was added to the CH_3COONa electrolyte solution to prepare the Na/Zn hybrid electrolyte, which can expand the ESW to 1.5 V.[130] The presence of Na^+ promotes the rapid deposition of Zn^{2+} in the electrolyte on the Zn anode, which can accelerate the occurrence of redox reactions, and endow Zn//NMTP batteries with appealing cycling stability and excellent discharge capacity (55.6 mA h g^{-1}) (Fig. 11e). Despite the many advantages of diluted electrolytes, they still face the problem of narrow ESW, resulting in side reactions such as the HER/OER, proton co-intercalation and active material dissolution, limiting their practical applications in energy storage systems.

4.2.2. Concentrated electrolytes. Compared with diluted electrolytes, the concentrated electrolytes can inhibit water decomposition, broaden the ESW, and optimize the performance of active materials, thereby reducing side reactions and increasing the energy density of ARSIBs. Using 5 M $NaNO_3$ solution as electrolyte, the ESW can be expanded to 1.9 V, but there is still a problem of material dissolution.[131] Na–bis(-fluorosulfonyl)imide (NaFSI) is easily soluble in water solution, and the ESW of 35 m NaFSI electrolyte is as high as 2.6 V, which improves the electrochemical performance of ARSIBs.[132] Normally, $NaClO_4$, which is a promising sodium salt in aqueous electrolytes, can be applied in concentrated electrolytes owing to their high solubility in aqueous solution, for high-performance ARSIBs. As shown in Fig. 11f, the NVTP@C//NVTP@C symmetrical battery exhibits outstanding rate performance and appealing cycle performance in 5 M $NaClO_4$ concentrated electrolyte, which can charge and discharge over 2500 times even at 10C.[133]

In previous reports, 17 m $NaClO_4$ WIS electrolytes have been widely used in high-voltage ARSIBs, in which the amount of free water is less than that of salt, and can expand the ESW to 3 V.[134–136] Furthermore, the 17 m $NaClO_4$ electrolytes can greatly inhibit water decomposition, reduce the side reactions of the HER/OER, and avert the structural collapse of active materials. As shown in Fig. 11g, the capacities of NaCuHCF, $Na_xCuCNPFe$, and $Na_xCuTolFe$ are 60, 41 and 36 mA h g^{-1} at 25 mA g^{-1} in 1 M Na_2SO_4 electrolyte, respectively. After cycling 2000 times in 1 M Na_2SO_4 dilute electrolyte, the capacity of $Na_xCuCNPFe$ and $Na_xCuTolFe$ decreased by half at 1 A g^{-1}, and the capacity of NaCuHCF decreased rapidly to 0%. Nevertheless, after 2000 cycles in 17 m $NaClO_4$ electrolyte, the capacities of NaCuHCF, $Na_xCuCNPFe$, and $Na_xCuTolFe$ are rarely reduced (Fig. 11h).[75] The above reason is that there is less free water in the concentrated electrolyte than in the dilute electrolyte, which effectively avoids side reactions during the reactions.

With the further development of concentrated electrolytes, in addition to conventional neutral electrolytes, 17 m $NaClO_4$ alkaline electrolytes also exhibit promising applications for ARSIBs. As shown in Fig. 11i, the rich OH^- in alkaline electrolyte creates an alkaline environment and inhibits the HER on the NTP anode. A layer of nickel/carbon nanoparticle (Ni/C) is coated on the $Na_2MnFe(CN)_6$ to form a H_3O^+-rich condition near the $Na_2MnFe(CN)_6$/Ni/C (NMF) cathode, which significantly inhibits the OER and causes the deterioration of electrode structure. Compared to ARSIBs with neutral electrolytes, NTP//NMF batteries with 17 m $NaClO_4$ alkaline electrolytes (include 1 M NaOH) present outstanding cycle performance over 13 000 cycles even at 10C (Fig. 11j).[137]

In summary, the concentrated electrolytes possess many advantages in expanding the ESW and inhibiting side reactions, which make it possible to develop the high-performance aqueous batteries at low cost, with safety and excellent cycling stability. However, some inevitable problems (such as high viscosity) still need to be resolved.

4.2.3. Low freezing point electrolytes. Due to its high conductivity, eco-friendliness, and safety, the aqueous

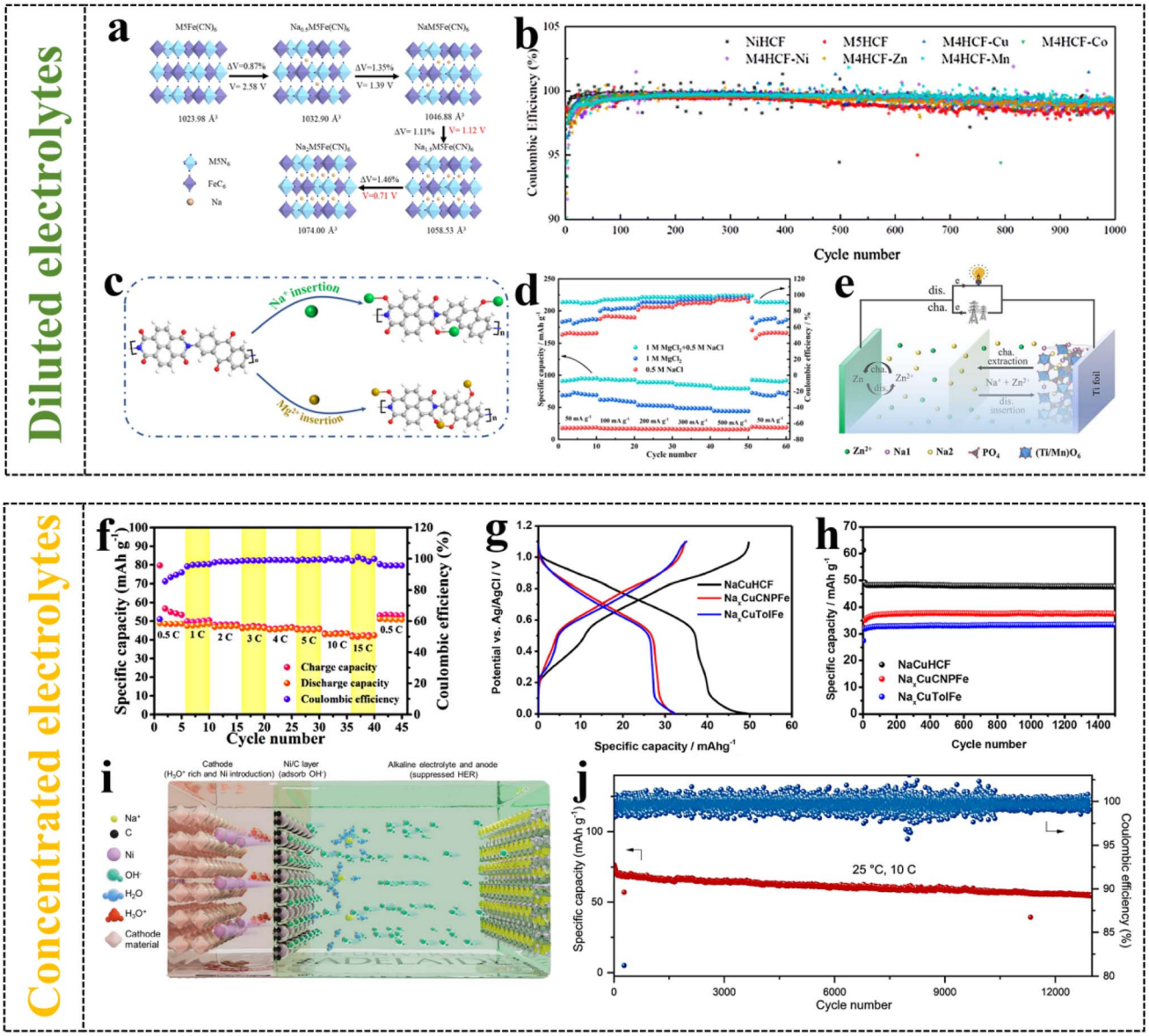

Fig. 11 (a) The discharging process for M5HCF. (b) CE of the samples.[116] (c) The insertion behavior of Mg^{2+}/Na^{+} in electrode materials. (d) Rate capability of the PNTAQ//MnO_2 battery.[127] Reproduced from ref. 127 with permission from John Wiley and Sons, copyright 2022. (e) Na/Zn hybrid ion batteries.[130] Reproduced from ref. 130 with permission from Elsevier, copyright 2021. (f) Rate capability of NVTP@C//NVTP@C.[133] Reproduced from ref. 133 with permission from the American Chemical Society, copyright 2021. (g) The voltage curves at 25 mA g^{-1}, (h) cycle performance in 17 m $NaClO_4$.[75] Reproduced from ref. 75 with permission from Elsevier, copyright 2022. (i) Reaction mechanism of the alkaline aqueous battery, (j) cycle life of the battery.[137] Reproduced from ref. 137 with permission from Springer Nature, copyright 2024.

electrolyte has gained increasing attention. Nevertheless, the high freezing points of aqueous electrolytes significantly limit the further applications of energy storage systems at low temperature. Each water molecule contains two hydrogen atoms and one oxygen atom, making water both a donor and acceptor of HBs. Moreover, water molecules are in a constant vibration state in the solution, and the HBs among water molecules are in a dynamic equilibrium state of formation and decomposition. As temperature decreases, the vibration of water molecules reduces, leading to the average probability of HB formation being greater than that of HB dissociation, thereby facilitating crystallization. Therefore, further research on aqueous electrolytes with a low freezing point is the primary task to expand the scope of application.

In recent years, the solvation effect has been used to prevent the aqueous electrolytes from freezing, the addition of additives in aqueous electrolyte can form new HBs, expanding the distance and destroying the connection between water molecules.[138] Typically, some organic solutions as co-solvents are added into the electrolytes to obtain low freezing point electrolytes, and the ESW can be significantly broadened. According to previous reports, dimethyl sulfoxide (DMSO),[139] acetonitrile (ACN),[140] methanol,[141] formamide (FA)[142] and ethylene glycol (EG)[143] have been explored as co-solvents for low-freezing-point electrolytes. The proportion

of water in the diluted electrolyte is larger than that of salt, and it is easy to crystallize at low temperature. DMSO can be mixed with water in any ratio and used as a receptor for HBs. An appropriate amount of DMSO was added to 2 M $NaClO_4$ solution as a co-solvent to get the mixed electrolyte with a freezing point of −50 °C (2 M-0.3 electrolyte).[139] At low temperature, the addition of DMSO destroys the original intermolecular HBs and forms a new HB network, thus avoiding the rapid crystallization and precipitation of the aqueous electrolyte (Fig. 12a). Moreover, the NTP//AC full battery shows great electrochemical performance in 2 M-0.3 electrolyte, and even at −50 °C, the battery capacity remains at 60% of the initial capacity at 25 °C (Fig. 12b).

At room temperature, WIS electrolytes resemble near-saturated salt solutions. However, at low temperatures, the solubility of the salt decreases, causing salt to crystallize and precipitate on the electrodes, thus reducing the energy density and cycle performance of ARSIBs. A mixed electrolyte was prepared by adding ACN as additive into 17 m $NaClO_4$ electrolyte, and shows a low freezing point. The Na^+ detaches from the cation–anion aggregates and coordinates with the ACN molecules, lowing the interactions among ions, thus preventing the precipitation of $NaClO_4$. The device works well even at −50 °C,[140] demonstrating excellent electrochemical performance and appealing stability. When FA is used as a co-solvent, FA molecules coordinate with water molecules to form new HBs, breaking direct connections between water molecules and preventing them from forming long-range ordered structures below 0 °C (Fig. 12c). Furthermore, the ARSIBs assembled with AC, organic polymer, and 17 m $NaClO_4$–FA electrolyte exhibit outstanding electrochemical performance and appealing cycling stability.[142] The specific capacity of the battery hardly drops at −50 °C after charging/discharging for 8000 cycles (Fig. 12d), and the battery can light up an LED and power a smartphone at −50 °C (Fig. 12e), demonstrating great application potential in ARSIBs.

A suitable additive for aqueous electrolytes should satisfy the needs of high polarity, high boiling points, and thermal stability, which should not only be miscible with water but also dissolve inorganic salts. The development of low-freezing-point aqueous electrolytes offers a valuable strategy for the advancement of high-performance ARSIBs. However, the dosage and reaction mechanisms of additives need to be further explored.

4.3. Hydrogel electrolytes

Hydrogel electrolytes are hydrophilic polymers composed of cross-linked polymer chains. Owing to their light weight, high

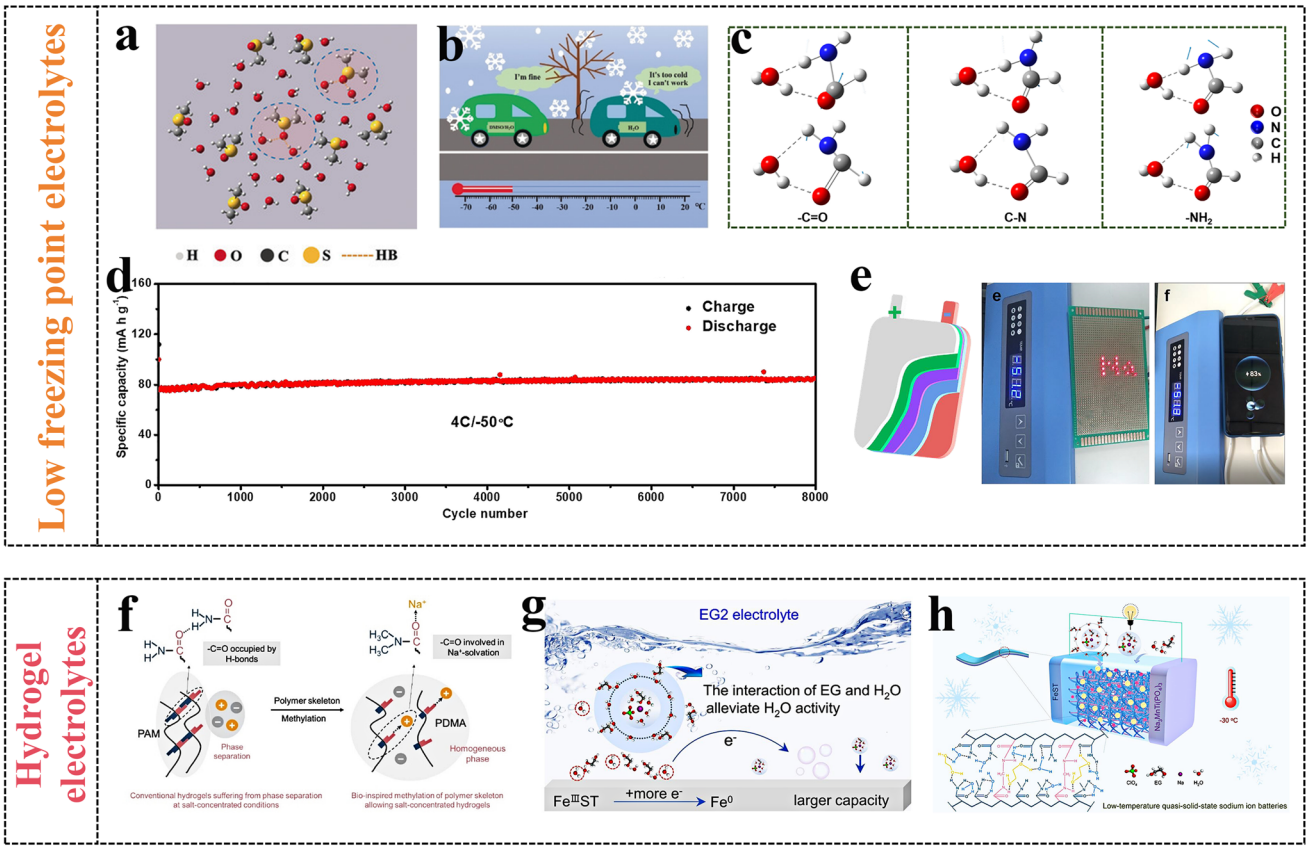

Fig. 12 (a) The result of MD simulations, (b) the effect of electrolyte additive DMSO.[139] Reproduced from ref. 139 with permission from John Wiley and Sons, copyright 2019. (c) Different functional groups among H_2O–FA clusters, (d) cycle performance, (e) the pouch cell can light LEDs and power a mobile phone at −50 °C.[142] Reproduced from ref. 142 with permission from Elsevier, copyright 2022. (f) Schematic illustration of the polymer structure.[148] Reproduced from ref. 148 with permission from John Wiley and Sons, copyright 2023. (g) Schematic diagram of the function mechanism of electrolyte additive EG, (h) electrochemical performance and mechanisms of the pouch cell at −30 °C.[149] Reproduced from ref. 149 with permission from Elsevier, copyright 2024.

safety and environmental friendliness, hydrogel electrolytes are promising in flexible electronics. Although liquid electrolytes have high conductivity and fast ion diffusion kinetics, they can reduce the flexibility of the devices. Under extreme conditions (such as bending, piercing, and cutting), flexible devices with liquid electrolytes are more vulnerable to external damage, resulting in electrolyte leakage and device failure. In contrast, the devices with hydrogel electrolytes not only possess excellent mechanical performance, but also eliminate the risk of electrolyte leakage, imparting better resistance to external damage.

Hydrogel electrolytes based on proton-conducting polymer matrices, such as polyacrylic acid, polyvinyl alcohol, polyacrylamide, and sodium alginate, are widely used in aqueous metal-ion (Li^+, Na^+, K^+, Zn^{2+}) batteries.[144–147] The NVP//NTP full battery with poly(*N*,*N*-dimethylacrylamide) (PDMA) hydrogel electrolyte exhibits excellent cycle performance, and its capacity retention is still at 82.8% after cycling 580 times at 2C (Fig. 12f).[148] As shown in Fig. 12g, an anti-freezing EG–PAM–$NaClO_4$ hydrogel electrolyte is prepared by using EG, polyacrylamide (PAM), and $NaClO_4$ concentrated electrolyte, and the addition of EG additives to the electrolyte can reduce HBs among solvent molecules, and form new HBs between EG and solvent molecules.[149] The interaction between EG and water combines with the synergistic effect of cross-linked polyacrylamide networks, effectively inhibiting water solidification in hydrogel electrolytes, maintaining superior water retention and showing significant mechanical extensibility at −40 °C. In addition, the anti-freezing hydrogel electrolytes, iron-incorporated sodium titanate (FeST) anode, and NMTP cathode are used to fabricate the flexible ARSIBs FeST//NMTP (Fig. 12h). These flexible batteries present high energy density (43.6 W h kg^{-1}), even at −30 °C, and the batteries can work well and a capacity retention of 64% can be achieved. Additionally, this flexible ARSIBs exhibit robust mechanical durability under bending and compression states, which can effectively power electronics at −30 °C. Although designing ultra-high conductivity hydrogel electrolytes needs further exploration, hydrogel electrolytes are still significant in the development of portable and flexible energy storage devices due to their high safety and excellent mechanical performance.

In summary, electrolytes are significant in the advancement of high-performance ARSIBs. Diluted electrolytes possess the advantages of excellent conductivity and low cost, but the narrow ESW (1.23 V) limits their wide applications. Concentrated electrolytes can expand the ESW to 3 V, as well as reducing the side reactions of the HER/OER, structural collapse of active materials and proton co-intercalation, thereby improving the energy density and cycling stability of the batteries. Nevertheless, there is also the problem of high viscosity of the electrolyte, make it easily crystallize at low temperature. Adding organic co-solvents as additives is a effective method of obtaining ARSIBs with low freezing point. By adjusting the solvation structure, the HBs between water molecules are broken, and new HBs between the co-solvent and water are formed, thereby endowing the electrolyte with anti-freezing performance and enhancing the energy density of the batteries. However, the dosage of additives and the reaction mechanism still need to be further explored. In addition, hydrogel electrolytes exhibit light weight, high safety and eco-friendliness, and the flexible ARSIBs with hydrogel electrolytes can achieve excellent electrochemical performance while maintaining high flexibility, which are promising for the advancement of flexible and wearable electronics. Nevertheless, it is essential to further explore high conductivity hydrogel electrolytes and more information about characteristics of the multiple electrolytes is shown in Table 1.

5. Flexible ARSIBs' structural design

The advancement of flexible, wearable, and even implantable electronics has resulted in the success of corresponding energy storage systems. Traditional ARSIBs are bulky, heavy, rigid, failing to satisfy the conditions of flexibility, light weight, and great biocompatibility for wearable electronics. In recent years,

Table 1 The summary of advantages, disadvantages, and applicable temperature for multiple electrolytes

	Advantages	Disadvantages	Common electrolyte (applicable temperature)	Ref.
Diluted electrolytes	High conductivity, low cost, high safety	Narrow voltage window, HER/OER side reaction	1 M Na_2SO_4 (25 °C)	116
			1 M $NaNO_3$ (25 °C)	118
			0.5 M CH_3COONa/$Zn(CH_3COO)_2$ (25 °C)	130
Concentrated electrolytes	Wide voltage window, high safety, superior stability	Low-cost effectiveness, high viscosity	9.26 m NaOTF (25 °C)	114
			17 m $NaClO_4$ + 1 M NaOH (25 °C)	137
			35 m NaFSI (25 °C)	132
Low freezing point electrolytes	Low freezing point, superior stability	Low-cost effectiveness	2 M $NaClO_4$/DMSO (−50–25 °C)	139
			17 m $NaClO_4$/ACN (−50–25 °C)	140
			17 m $NaClO_4$/FA (−50–25 °C)	142
Hydrogel electrolytes	Low freezing point, superior stability	Low-cost effectiveness	PDMA hydrogel electrolyte (25 °C)	148
			EG–PAM–$NaClO_4$ hydrogel electrolyte (−30–25 °C)	149

the studies on flexible aqueous LIBs, Zn-ion batteries, and Al-ion batteries have been extensive, and those batteries have already been applied in wearable electronics, but there have been few studies on flexible ARSIBs.[150–152] The flexible ARSIBs possess abundant Na resources, biocompatibility, safety, and appealing mechanical performance, in accord with the requirements of flexible, wearable and implantable electronics. In addition to electrode materials and electrolytes, the structural design of batteries is also crucial to their performance and applications. To this end, the flexible ARSIBs are categorized based on their structural design into fiber-based, paper-based, metal current collector-based, and self-supporting batteries, with a detailed analysis and summary.

5.1. Fiber-based flexible ARSIBs

Different from conventional planar flexible energy storage devices, flexible fiber-based energy storage devices without current collectors and conductive additives not only exhibit high energy density and excellent cycle performance, but also satisfy the needs of flexibility and light weight for wearable electronics. The manufacture of fiber-based flexible electrodes is the priority of flexible fiber-based energy storage devices. Metal wires, CNFs, polymer fibers, and CNTs have been used to prepare flexible fiber-based batteries and capacitors.[153–155] For example, CNTs have high flexibility, tensile strength, and high conductivity, which show promise for application as current collectors for flexible fiber-based electrodes. In Fig. 13a, the CNTs were coated with $NaTi_2(PO_4)_3$@C (NTPO@C) and $Na_{0.44}MnO_2$ active materials, which were twisted into fibrous electrodes, thus fabricating the NTPO@C//$Na_{0.44}MnO_2$ fiber-based flexible ARSIBs.[18] As shown in Fig. 13b, the prepared NTPO@C//$Na_{0.44}MnO_2$ fiber-based flexible ARSIBs show appealing cycle performance in 1 M $NaSO_4$ electrolytes, and the capacity retention of the battery can reach 76% after 100 cycles. Moreover, even after bending at 180° for 100 cycles, the capacity of the battery hardly decreased, and the cycle performance of the battery barely changed (Fig. 13c), indicating that the fiber-based ARSIBs possess excellent electrochemical performance and phenomenal mechanical performance. To further explore the application range of fibrous ARSIBs the electrochemical performance of the batteries was tested in saline and cell-culture medium, and the discharge capacities of these

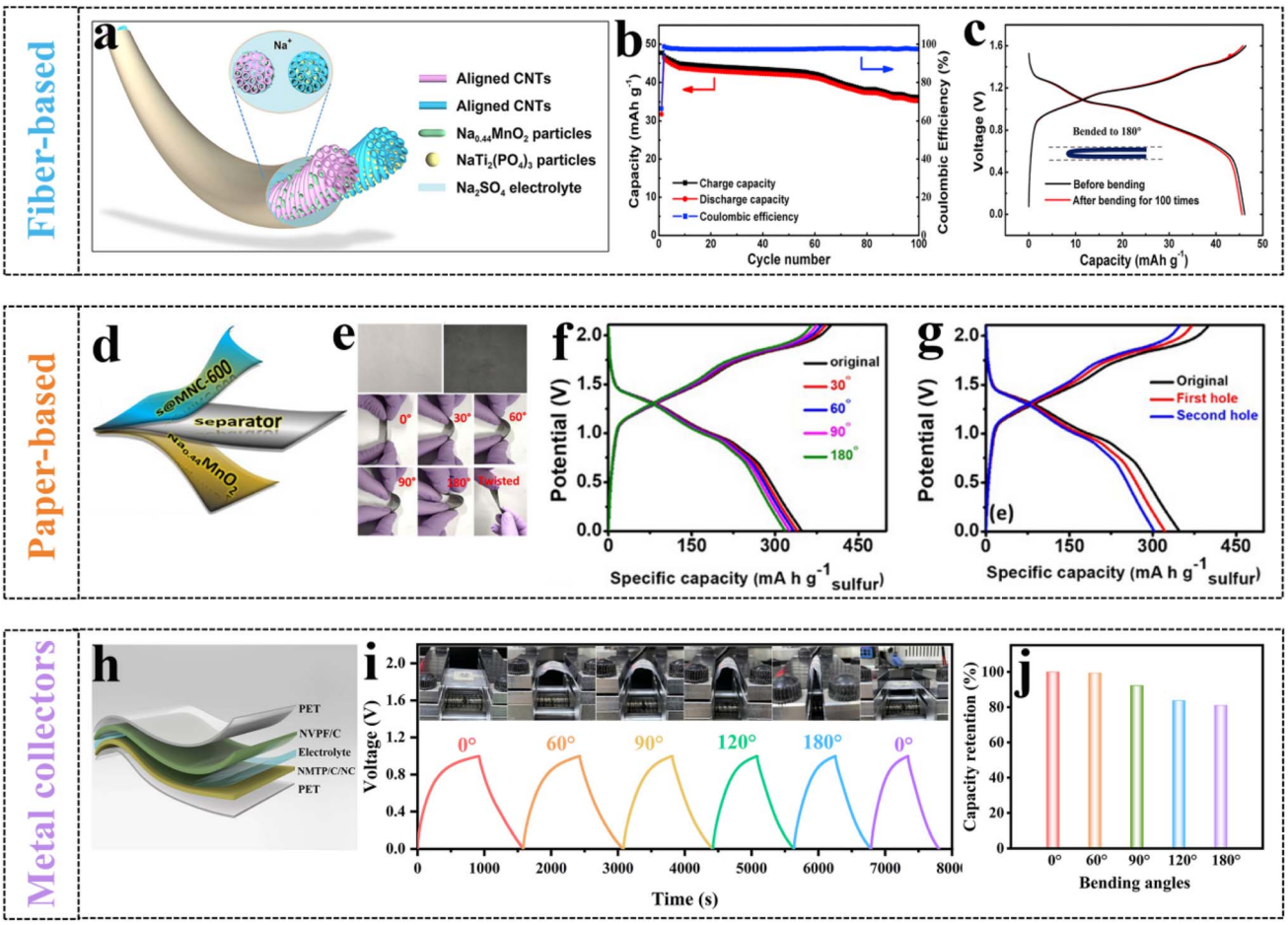

Fig. 13 (a) Schematic diagram of the fibrous battery, (b) cycle performance, (c) the voltage curves of the batteries.[18] Reproduced from ref. 18 with permission from Elsevier, copyright 2017. (d) Schematic representation of paper-based flexible ARSIBs, (e) the state of the paper-based flexible battery at various angles, the capacities of the battery (f) under bending states and (g) after punching holes.[22] Reproduced from ref. 22 with permission from Elsevier, copyright 2022. (h) Schematic representation of fully-printed ARSIBs, (i) and (j) the electrochemical performance of the battery under bending states.[24] Reproduced from ref. 24 with permission from John Wiley and Sons, copyright 2024.

batteries still remained at 37 mA h g^{-1} and 32 mA h g^{-1}, respectively, demonstrating great biocompatibility and appealing stability. Fiber-based flexible ARSIBs with high energy density, outstanding mechanical performance, appealing stability and great biocompatibility are promising in practical applications of wearable and implantable electronics.

5.2. Paper-based flexible ARSIBs

Paper-based flexible energy storage devices can be employed in wearable electronics due to the abundant resources, high flexibility, and biocompatibility.[26,156] The fibers in paper possess strong intermolecular and intramolecular HBs, endowing paper-based electrodes with appealing mechanical performance. The large specific surface area and porous structure enable the paper to absorb more electrolytes through capillary action, allowing for a greater number of extensive interactions between the electrolytes and active materials. Paper-based flexible ARSIBs serve as an appealing energy system that holds promise in the development of wearable electronics. Using paper as a flexible substrate for ARSIBs typically involves incorporating conductive carbon materials to improve their conductivity, such as CNTs, CNFs, and graphene. For example, S@C, $Na_{0.44}MnO_2$, Nafion membrane, graphite paper current collector, and 17 m $NaClO_4$ electrolyte were used to assemble the paper-based flexible ARSIBs S@C//$Na_{0.44}MnO_2$ (Fig. 13d).[22] The flexible battery delivers excellent capacity (348 mA h g^{-1}), phenomenal rate performance and appealing Na^+ storage performance. Furthermore, under different bending angles, the capacity of the battery decays very little (Fig. 13e and f), and even after punching holes on the battery, the electrochemical performance is rarely affected (Fig. 13g), proving excellent mechanical performance and appealing stability. These paper-based electrodes with ultra-small resistance and volume hold promise for achieving both high power density and energy density simultaneously.

5.3. Flexible ARSIBs with metal collectors

Owing to the superior conductivity and high flexibility, metal foils (copper, aluminum, and titanium) used as conductive current collectors for electrodes have gained widespread utilization in flexible energy storage devices.[157–159] As is well known, silver foil, despite its excellent conductivity, suffers from poor mechanical performance, rendering it unsuitable as a current collector for flexible devices. Interestingly, the silver current collector is prepared by printing silver paste on a polyethylene terephthalate substrate *via* the screen-printing technique, which presents high conductivity and excellent mechanical performance. As shown in Fig. 13h, the first fully printed

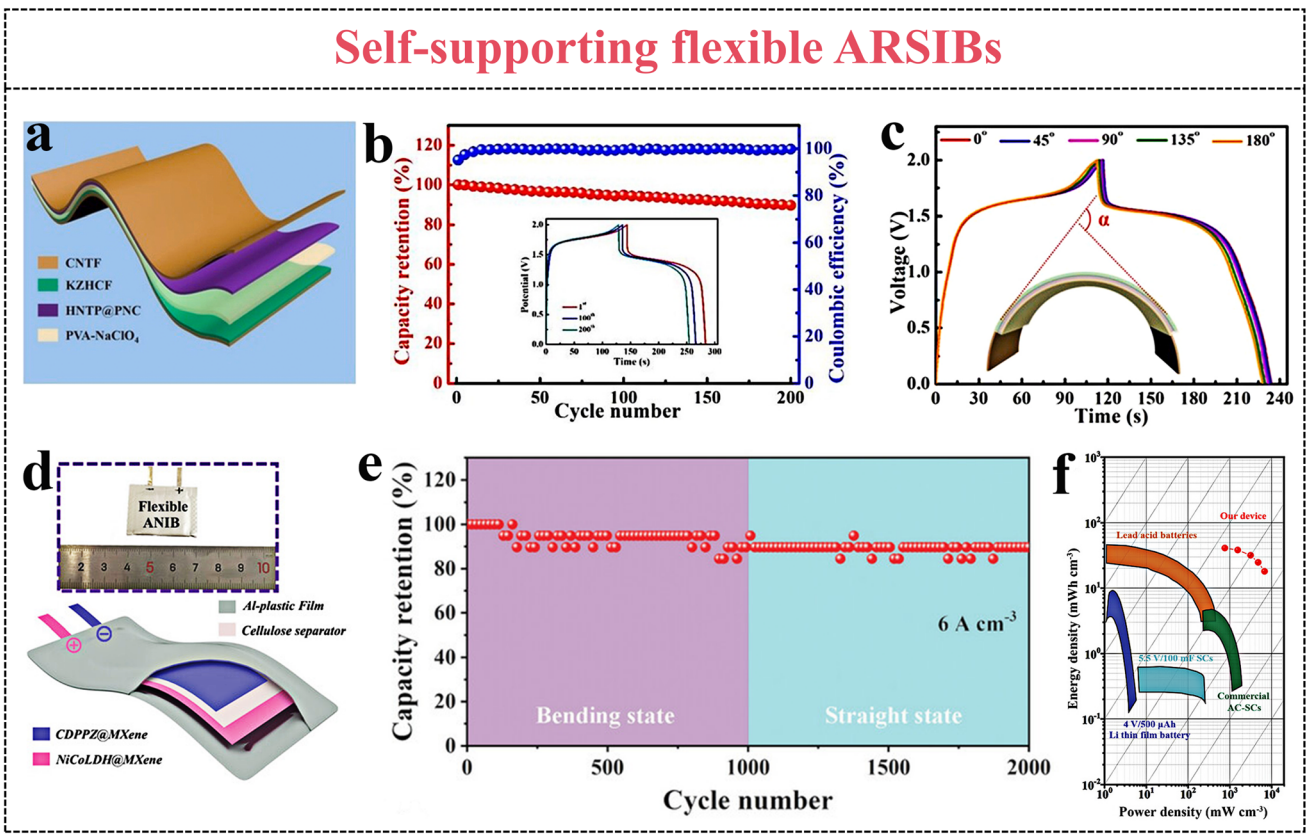

Fig. 14 (a) Schematic illustration of self-supporting flexible ARSIBs, (b) cycle performance, (c) the voltage curves of the HNTP@PNC//CNTF@KZHCF battery under different bending angles.[21] Reproduced from ref. 21 with permission from Elsevier, copyright 2021. (d) The soft-package flexible ARSIBs, (e) cycle performance, (f) comparison between the energy density of various energy storage devices.[23] Reproduced from ref. 23 with permission from John Wiley and Sons, copyright 2023.

flexible ARSIBs were obtained by the screen-printing technique, including the printed $Na_3V_2(PO_4)_2F_3$/C (NVPF/C) cathode, Na_3-$MnTi(PO_4)_3$/C with 2% nitrogenous carbon (NMTP/C/NC) anodes, and printed electrolytes.[24] The metal collectors with the advantages of high conductivity and outstanding mechanical performance endow the batteries with excellent energy density (40.1 W h kg^{-1}), high flexibility and stability. Furthermore, the capacity retention of this flexible battery still remains at 81% even after bending at 180° for 200 cycles (Fig. 13i and j). This fully-printed battery enables miniaturization, integration, and patterning, showing outstanding mechanical performance and excellent electrochemical performance. The structural design and manufacturing technique of the fully-printed batteries can offer a new perspective for the advancement of flexible and wearable electronics.

5.4. Self-supporting flexible ARSIBs

Flexible electrodes are typically composed of active materials, current collectors, binders, and conductive carbon materials. However, the weight and volume of the electrodes are increased as a result of the addition of current collectors and binders, thereby reducing the mass specific capacity of the batteries. The self-supporting flexible electrodes are free of current collectors, binders and conductive carbon materials, exhibiting excellent energy density and appealing flexibility.[160,161] Generally, active materials are attached to carbon cloth or conductive carbon material arrays to prepare conductive films as self-supporting flexible electrodes.

The hollow-structure $NaTi_2(PO_4)_3$ nanoparticles (HNTP) were embedded in porous N-doped carbon nanofiber (PNC) arrays by electrospinning to prepare HNTP@PNC flexible anodes. Moreover, potassium zinc hexacyanoferrate (KZHCF) materials are loaded on CNT films to obtain CNTF@KZHCF flexible cathodes (Fig. 14a).[21] The HNTP@PNC//CNTF@KZHCF battery exhibits appealing cycle performance, the discharge capacity still remains at 89.6% of its initial capacity, and the CE can reach 100% (0.48 A cm^{-3}) after 200 cycles (Fig. 14b). Moreover, the capacity of the flexible battery decreases little at 45°, 90°, 135°, and 180° bending states; even upon bending at 90° for 500 cycles, the capacity remains at 89.8% of the initial capacity (Fig. 14c). The self-supporting flexible ARSIBs show excellent mechanical performance and phenomenal stability, offering a development direction for flexible electronics.

As a 2D transition metal carbide and nitride, MXene provides abundant covalent bonds and ionic bonds, leading to excellent conductivity and high hydrophilicity, which is promising as a flexible electrode material. A carboxyl-substituted dipyridophenazine (CDPPZ) suspension was fully mixed with MXene solution to fabricate porous, conductive and flexible MXene@CDPPZ composite films, as a flexible self-supporting anode. The NiCoLDH@MXene composite films were prepared as a flexible self-supporting cathode by the same method. As shown in Fig. 14d, the anodes and cathodes and 10 M NaOH electrolytes were vacuum-encapsulated in aluminum–plastic film to form soft-package flexible ARSIBs.[23] The discharge capacity of the battery decreases little under different bending states (0–120°),

Table 2 The summary of flexible ARSIBs with different flexible current collector structures

Battery	System	Working window	Capacity (capacity/current density)	Cycle performance (cycles/capacity retention)	Mechanical performance (bending angle/cycles/capacity retention)	Ref.
NTPO@C//$Na_{0.44}MnO_2$	Fiber-based flexible ARSIBs	0–1.6 V	43 mA h g^{-1}/0.1 A g^{-1}	100/76%	180°/100/88%	18
S@C//$Na_{0.44}MnO_2$	Paper-based flexible ARSIBs	0–1.6 V	94.3 mA h g^{-1}/0.5C	300/82%	60°/100/65%	22
NMTP/C/NC//NVPF/C	Flexible ARSIBs with a metal collector	0–1 V	40.1 mA h g^{-1}/0.1C	100/78%	180°/200/81%	24
HNTP@PNC//CNTF@KZHCF	Self-supporting flexible ARSIBs	0.6–1.9 V	24.5 mA h cm^{-3}/0.04 A cm^{-3}	200/89.6%	90°/500/89.8%	21
MXene@CDPPZ//NiCoLDH@MXene	Self-supporting flexible ARSIBs	0–1.6 V	51.2 mA h cm^{-3}/6 A cm^{-3}	2000/91%	120°/1000/91%	23

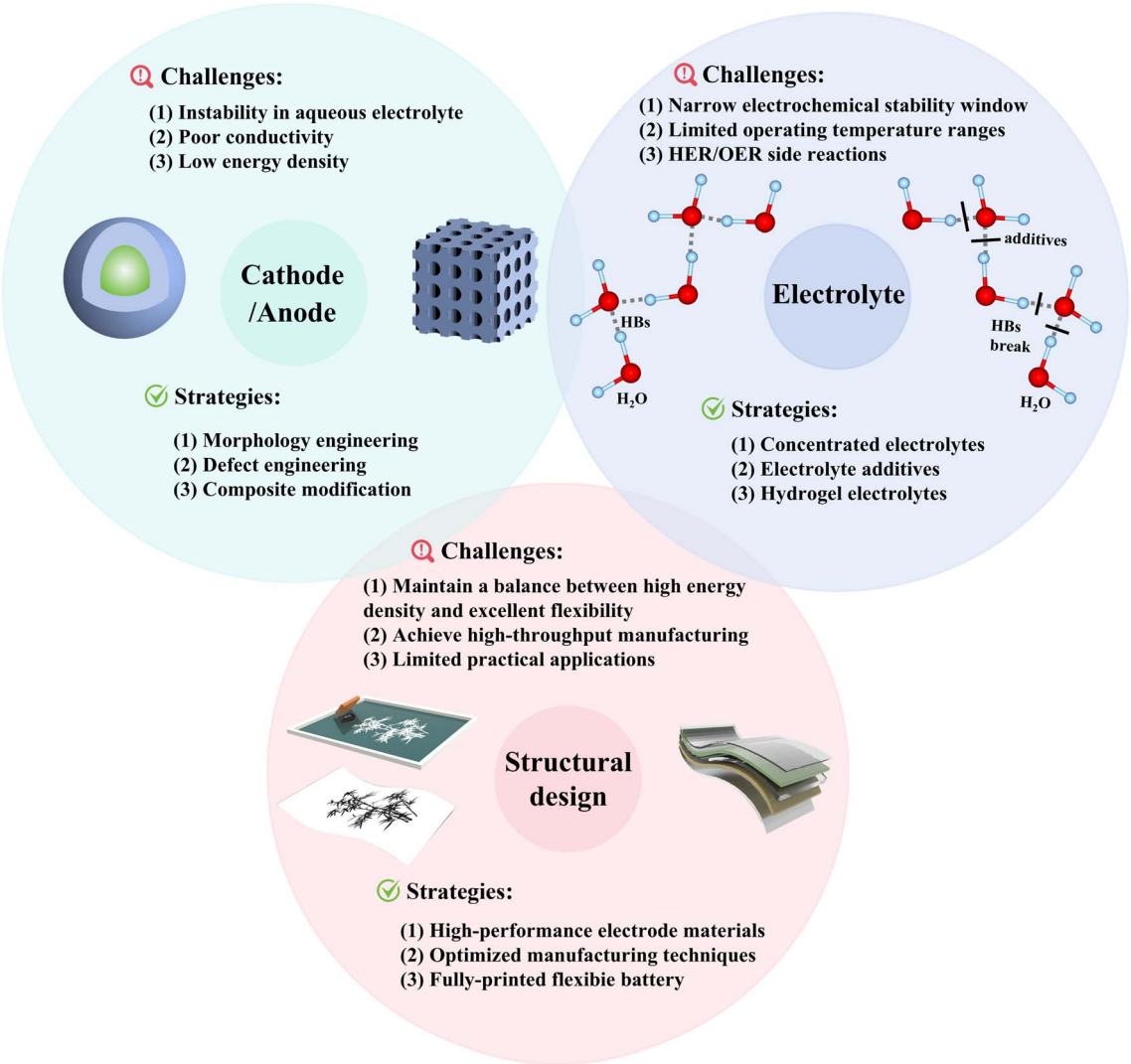

Fig. 15 The challenges and strategies with respect to the cathode, anode, electrolyte, and structural design of flexible ARSIBs.

demonstrating phenomenal electrochemical performance, and appealing flexibility (Fig. 14e). Furthermore, this battery can power an electronic clock whether at flat or bending states, and its performance even surpasses that of commercial lithium iron phosphate and lithium-ion batteries (Fig. 14f).

According to the structural designs, functional flexible ARSIBs including fiber-based, paper-based, metal current collector-based, and self-supporting ARSIBs are developed to meet the requirements of flexible electronics. Table 2 summarizes the reported flexible ARSIBs with the different structural designs of flexible current collectors. Flexible ARSIBs with the advantages of safety, low cost and flexibility are essential in the advancement of wearable electronics. In addition, Fig. 15 summarizes the challenges and key strategies with respect to the cathode, anode, electrolyte, and structural design, providing valuable information for the development of high-performance flexible ARSIBs. In summary, it is significant to optimize active materials and electrolytes, and improve structural design for achieving a balance between energy density and functionality in ARSIBs.

6. Applications of flexible ARSIBs

6.1. Flexible energy systems for portable electronics

The flexibility, lightweight, and biocompatibility characteristics are identified as essential design criteria for flexible energy systems in wearable electronics, ensuring the safety and comfort of these devices during wearing. Compared to conventional LIBs and SIBs, flexible ARSIBs can be widely used in wearable electronic devices, because of their low cost, safety, eco-friendliness, flexibility, and biocompatibility (Table 3). As shown in Fig. 16a, perylene tetracarboxylic diimide (PTCDI) nanofibers are constructed onto flexible indium tin oxide films, thereby fabricating a binder-free PTCDI-nano-organic anode. The aqueous flexible sodium ion storage devices (AFSISD) with a sandwich structure are assembled by combining the PTCDI-nano-organic anode with an activated carbon cathode and polyvinyl alcohol–Na_2SO_4 (PVA–Na_2SO_4) gel–electrolyte. This battery provides an excellent gravimetric energy density of 83.8 W h kg^{-1} and a power density of 3.4 kW kg^{-1}, and it can light up

Table 3 The summary of advantages and challenges for the various batteries

Battery	Advantages	Challenges
Flexible ARSIBs	High flexibility Low cost Safety Environmental friendliness	Low energy density HER/OER side reactions
Aqueous SIBs	Low cost Safety Environmental friendliness	Low energy density Poor flexibility HER/OER side reactions
SIBs	Low cost Long cycle life	Unsafe Poor flexibility
Aqueous LIBs	Safety Environmental friendliness	Low cost-effectiveness Low energy density HER/OER side reactions Poor flexibility
LIBs	High energy density Long cycle life Mature manufacturing technology	Low cost-effectiveness Unsafe Poor flexibility

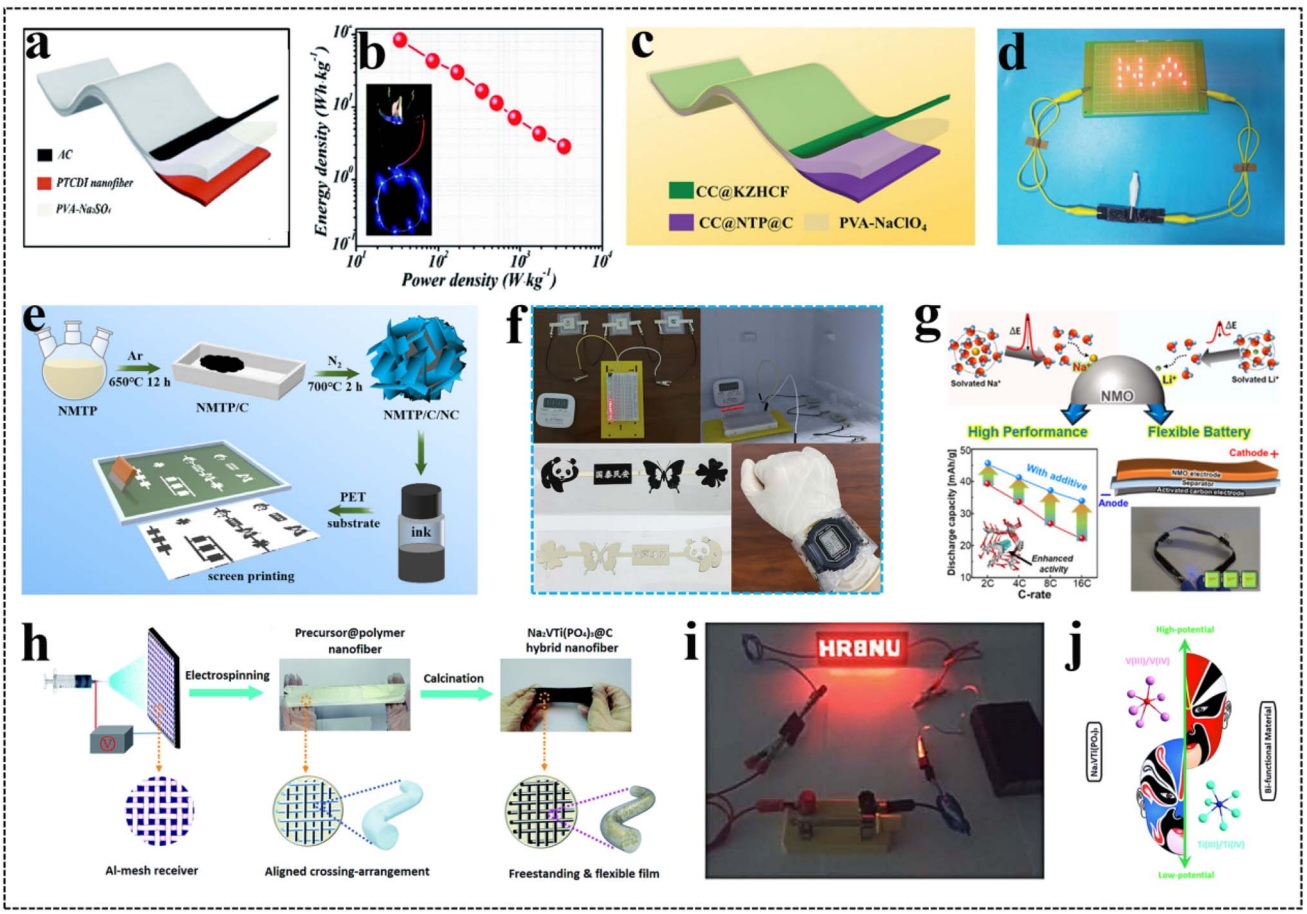

Fig. 16 (a) Schematic illustration and (b) electrochemical performance of AFSISD.[20] (c) Schematic illustration of the flexible ARSIBs, (d) two batteries connected in series can power 18 LEDs.[19] Reproduced from ref. 19 with permission from John Wiley and Sons, copyright 2019. (e) The preparation process of fully printed flexible electrodes, (f) the batteries can light LEDs and power an electronic watch.[24] Reproduced from ref. 24 with permission from John Wiley and Sons, copyright 2024. (g) Schematic illustration of the structure of the triple-stacked flexible battery.[128] Reproduced from ref. 128 with permission from the American Chemical Society, copyright 2020. (h) The synthesis of the NVTP/C hybrid nanofibers film, (i) the cross-linked nanofiber film can be used as a connector component in LED circuits, (j) schematic illustration of flexible symmetric ARSIBs.[162]

a ring LED strip even in the bent state (Fig. 16b).[20] Utilizing a zinc nanosheet as both the zinc source and reducing agent, a micro-cube-like $K_2Zn_3(Fe(CN)_6)_2 \cdot 9H_2O$ is grown on carbon cloth (CC) to fabricate the flexible cathode CC@KZHCF, and the flexible anode CC@NTP@C is fabricated by growing NTP onto CC. As shown in Fig. 16c, the flexible ARSIBs with a high output voltage platform are fabricated by the CC@KZHCF cathode and CC@NTP@C anode, which exhibit excellent energy density and attractive mechanical performance. In addition, two batteries connected in series can power 18 LEDs (Fig. 16d).[19] As shown in Fig. 16e, the fully-printed ARSIBs NMTP/NC//NVPF/C are fabricated using the screen printing technique, exhibiting excellent electrochemical performance and remarkable mechanical performance. Batteries with different patterns can be integrated in series and parallel to output the required voltage and capacity, which can light up 10 LEDs and serve as an energy bracelet to power an electronic watch (Fig. 16f).[24]

Other cations (such as Li^+ and Zn^{2+}) were introduced into the Na^+ electrolyte to prepare flexible aqueous hybrid-ion batteries, which present excellent electrochemical performance. For example, the addition of $LiNO_3$ to a Na_2SO_4 electrolyte enables the co-intercalation of Li^+ and Na^+, enhancing the performance of the sodium manganese oxide cathode. A triple-stacked flexible aqueous sodium/lithium hybrid-ion battery, comprising activated carbon and $Na_{0.39}MnO_2$, was integrated into an energy band that can power LEDs whether in a flat or bent state (Fig. 16g).[128] As shown in Fig. 16h, the NVTP/C hybrid nanofibers were prepared by an electrospinning method, which are well-aligned along two intersecting directions, forming flexible films with 3D network structure. The films with cross-linked architecture exhibit appealing flexibility, excellent stability, and high conductivity, which can serve as a connector component in LED circuits (Fig. 16i). Additionally, flexible self-supported symmetric ARSIBs NVTP/C//NVTP/C without binders, conductive additives, and current collectors present excellent electrochemical performance and high flexibility (Fig. 16j).[162]

Although flexible ARSIBs have been widely used in certain small, portable wearable electronics, their electrochemical performance still requires further enhancement while maintaining excellent flexibility. Further development is required to advance the applications of these flexible ARSIBs, particularly in integrating these batteries with small energy conversion devices to form integrated electronic systems. For example, combining flexible ARSIBs with flexible sensors, solar cells, wind power generators, and triboelectric nanogenerators can create a wearable integrated system.

6.2. Stability under extreme conditions

6.2.1. Waterproof performance. To achieve large-scale practical applications, it is crucial to explore flexible ARSIBs that can resist extreme conditions in complex environments. Under extreme conditions such as rain, swimming, and washing, the waterproof performance of flexible ARSIBs relies on the advanced packaging technologies, while also maintaining excellent flexibility. As shown in Fig. 17a, the flexible film is prepared by the active material ($Na_{0.44}MnO_2$ and NTP@C), conductive agent (acetylene black), binder (polytetrafluoroethylene), and isopropyl alcohol, and the film is pressed onto a stainless steel weld mesh to fabricate flexible film electrodes. Moreover, a separator soaked with electrolyte is placed between the anode and cathode to fabricate the flexible strip-shaped ARSIBs, and the batteries are sealed through a vacuum sealing process to ensure promising waterproof performance (Fig. 17b).[18]

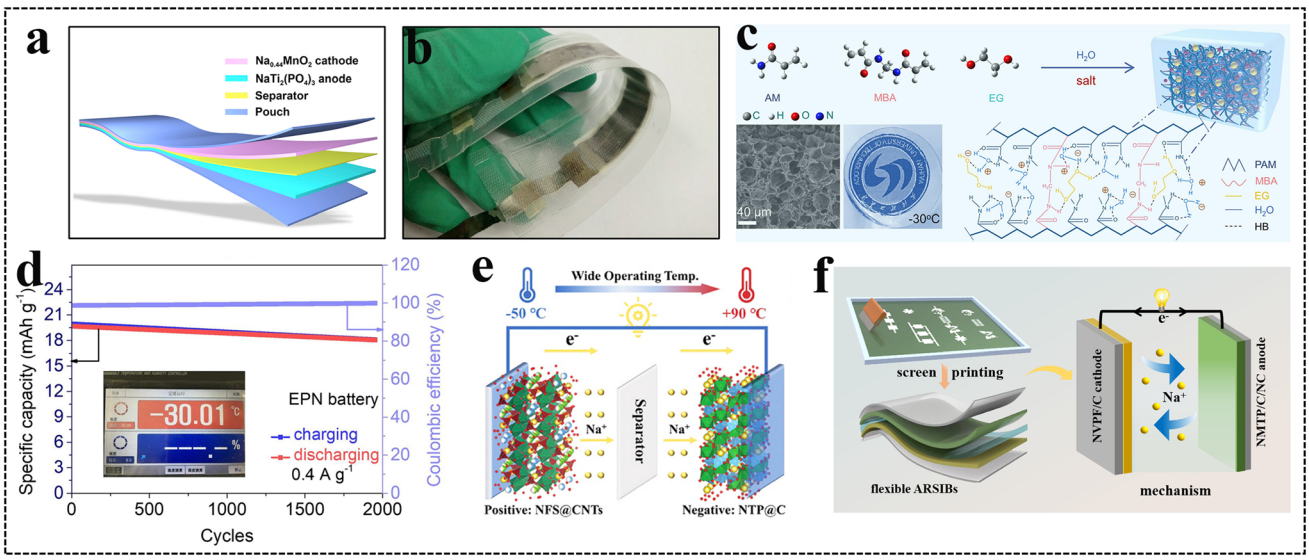

Fig. 17 (a) Schematic illustration of the flexible ARSIBs, (b) the photo of flexible strip-shaped ARSIBs.[18] Reproduced from ref. 18 with permission from Elsevier, copyright 2017. (c) The synthesis and mechanism of EPN hydrogel electrolyte, (d) electrochemical performance of the battery at −30 °C.[149] Reproduced from ref. 149 with permission from Elsevier, copyright 2024. (e) Schematic illustration of the NTP//NFS battery.[163] Reproduced from ref. 163 with permission from John Wiley and Sons, copyright 2024. (f) The structure and mechanism of fully-printed flexible ARSIBs.[24] Reproduced from ref. 24 with permission from John Wiley and Sons, copyright 2024.

6.2.2. Low/high temperature tolerance. Developing wide temperature flexible ARSIBs promotes practical applications, especially for special applications such as electric vehicles and extreme environment exploration. Electrolytes are most significantly affected at both low/high temperatures, especially aqueous electrolytes in practical applications. At low temperature, the electrolyte is easy to crystallize on the electrode, resulting in the decrease of ion-diffusion kinetics and deterioration of electrochemical behavior. As shown in Fig. 17c, an anti-freezing ethylene glycol–polyacrylamide–$NaClO_4$ (EPN) hydrogel electrolyte was synthesized using acrylamide as the monomer, methylene-bis-acrylamide as the crosslinker, $K_2S_2O_8$ as the initiator, $NaClO_4$ solution as the electrolyte, and EG as the additive. The addition of EG facilitates the formation of numerous HBs in the hydrogel electrolyte, even at −30 °C; this hydrogel electrolyte remains unfrozen, preserving its structural and functional integrity. Moreover, the anti-freezing battery FeST//NMTP with the EPN hydrogel electrolyte exhibit excellent electrochemical performance and high flexibility. After 1950 cycles at −30 °C, the capacity of the battery can remain at approximately 86% of its initial capacity and the CE can remain at 100% (Fig. 17d).[149]

High temperatures can exacerbate the instability of electrode materials and electrolytes. In aqueous electrolytes, solvents evaporate easily under high-temperature conditions, resulting in poor energy density and short cycle life. The development of stable electrode materials and appropriate electrolyte additives is crucial for achieving SIBs with low/high temperature tolerance. As shown in Fig. 17e, the high-performance SIBs NTP//$Na_{2.4}Fe_{1.8}(SO_4)_3$ (NTP//NFS) are fabricated with the stable $Na_{2.4}Fe_{1.8}(SO_4)_3$ (NFS) cathode, NTP anode, and ester-based electrolyte. These batteries demonstrate an ultra-long cycle life, and the capacity retention can remain at 70.7% after charging/discharging 10 000 times at 10C. Due to the high voltage platform and excellent stability of NTP and NFS in ester-based electrolytes, the full battery can work safely between −50 °C and 90 °C.[163] The stable electrode materials and appropriate electrolyte additives play a significant role in the design of wide-temperature ARSIBs.

6.2.3. Damage tolerance. Flexible ARSIBs are promising energy storage systems for portable wearable electronics. However, there is inevitable external damage in practical applications such as hammering, tearing, and puncturing. Therefore, ensuring the safety and resistance against damage of these batteries during use is necessary. In Fig. 17f, the fully printed flexible ARSIBs are assembled with the NVPF/C cathode, NMTP/NC anode, and 17 m $NaClO_4$/ethylene glycol (17 m $NaClO_4$–EG) electrolyte. The prepared battery was placed in a nylon/polyethylene vacuum-sealed pouch and secured using a vacuum heat-sealing machine. This battery exhibits excellent electrochemical performance and appealing mechanical performance under bending states of 180°. Furthermore, even when the battery is cut with a 1 cm slit, the capacity of the damaged battery hardly decreased.[24] Therefore, it is significant to develop flexible ARSIBs that resist extreme conditions for the advancement of portable wearable electronics.

7. Conclusions and outlook

Flexible ARSIBs have great potential for application in portable and wearable electronics due to their low cost, superior mechanical properties, environmental friendliness, and excellent electrochemical performance. The active materials, electrolytes, and structural design are of great significance for the development of flexible ARSIBs with both high energy density and multi-functionality, which have attracted extensive attention. This review introduces and discusses the latest developments in active materials and electrolytes in ARSIBs. The performance of active materials can be enhanced through optimization strategies such as morphology engineering, defect engineering, and composite modification, thereby obtaining high-performance ARSIBs. Furthermore, it is crucial to develop stable active materials with high performance and eco-friendliness, as well as low-cost aqueous electrolytes with a wide ESW and high stability. However, more research is still needed to fully understand the reaction mechanism of ARSIBs and to elucidate their performance enhancement mechanism. In addition, the recent progress of flexible ARSIBs based on fibers, paper, metal current collectors and self-supporting electrodes is also reviewed. These studies offer insightful analysis and helpful recommendations for the success of flexible and wearable electronics. More importantly, the practical applications of ARSIBs still need to be further explored.

(1) As an essential component of the battery, the development of high-performance active materials is essential to enhance ARSIB performance. So far, the most promising active materials in ARSIBs are metal oxides, polyanionic compounds, and PBAs, MOFs, and organic polymer materials. However, the instability, poor conductivity and low energy density of active materials in aqueous solution severely limit the advancement of high-performance ARSIBs. Optimization and improvement strategies such as morphology engineering, defect engineering, and composite modification are expected to enhance the performance of active materials. Morphology engineering aims at improving performance by altering the morphologies of the materials, which requires precise control over the structure and surface modification. The purpose of defect engineering is to optimize electrode materials by introducing defects on the surface and inside of the materials, but it is necessary to avoid excessive defects that could destroy the stability of the material and lead to structural collapse during the charging/discharging process. The fabrication of composite materials can improve the electrochemical performance of electrode materials, but it still faces challenges in the complex preparation process and the unclear interactions between materials. Hence, future research on innovative active materials and selecting appropriate optimization strategies is needed, according to specific requirements and practical applications for promoting the development of ARSIBs.

(2) Electrolytes are also an important component of the batteries, so it is a valuable research direction to develop suitable aqueous electrolytes for ARSIBs. So far, dilute electrolytes, concentrated electrolytes, and hydrogel electrolytes have been

widely reported. However, they still face the challenges of narrow ESW, limited operating temperature ranges, and side reactions (HER/OER, proton co-intercalation, and active material structure collapse). Moreover, the organic additives used to optimize the aqueous electrolytes still involve the risk of combustion, and the reaction mechanism needs to be further explored. Therefore, further exploration of novel electrolytes and optimization of reported electrolytes are necessary to obtain the high-performance ARSIBs.

(3) The success of high-performance flexible ARSIBs provides significant implications for their commercial viability. To attain this objective, there are multiple aspects that should be considered, such as optimizing electrode materials, developing aqueous electrolytes with a wide ESW, and exploring new design strategies. In addition, the comprehensive understanding of their energy storage mechanisms is necessary to fully utilize the potential of active materials. However, the current research on the reaction mechanism of ARSIBs is not clear enough. Additional computational simulations and more *in situ* characterization techniques are needed to investigate the reaction mechanism of ARSIBs and enhance their electrochemical performance.

(4) To achieve environmental sustainability goals, the recycling technology of active materials needs further improvement, and the development of biodegradable and eco-friendly materials as next-generation electrode materials is promising. Additionally, the application of flexible ARSIBs requires further expansion. On the one hand, these batteries can be integrated with small energy conversion devices (such as flexible sensors, solar cells, wind power generators, and triboelectric nanogenerators) to create wearable integrated electronic systems. On the other hand, further research into battery assembly and improvement strategies is needed to address the extreme conditions that flexible ARSIBs may encounter, such as high temperatures, high pressures, high salinity, low temperatures, and vacuum environments.

(5) Despite the great progress of aqueous metal ion batteries, the energy density is still lower than that of conventional organic batteries. Due to the advantages of safety, eco-friendliness and low cost, it is significant to explore new manufacturing techniques to prepare flexible ARSIBs with excellent flexibility and high performance. In recent years, screen-printing techniques have shown many advantages in the preparation of multifunctional flexible energy storage devices, including fully-printed flexible aqueous metal ion batteries and supercapacitors. The advantages of miniaturization, high flexibility, the tunability of shapes and sizes, and integration make them promising in portable, wearable, and flexible electronics.

Data availability

No primary research results, software or code have been included and no new data were generated or analysed as part of this review.

Author contributions

Hehe Ren: writing-original draft, writing-review & editing, visualization, software, investigation, formal analysis. Xinzhan Du: conceptualization, validation. Jing Liang: writing-review & editing, methodology, funding acquisition, data curation. Wei Wu: writing-review & editing, supervision, resources, project administration, funding acquisition.

Conflicts of interest

There are no conflicts to declare.

Acknowledgements

This work was supported by the National Natural Science Foundation of China (NSFC, Grant No. 52373252), the Fundamental Research, Key Research and Development Project of Hubei Province (2022BCA040), and China Postdoctoral Science Foundation (2022TQ0239, 2022M722465).

References

1 M. Li, J. Lu, Z. Chen and K. Amine, *Adv. Mater.*, 2018, **30**, 1800561.
2 J. B. Goodenough, *Nat. Electron.*, 2018, **1**, 204.
3 P. Poizot, S. Laruelle, S. Grugeon, L. Dupont and J. M. Tarascon, *Nature*, 2000, **407**, 496–499.
4 Y. Chen, T. Wang, H. Tian, D. Su, Q. Zhang and G. Wang, *Adv. Mater.*, 2021, **33**, 2003666.
5 P. K. Nayak, L. Yang, W. Brehm and P. Adelhelm, *Angew. Chem., Int. Ed.*, 2017, **57**, 102–120.
6 Y. Wang, D. Liu, M. Sun and J. Liu, *Mater. Chem. Front.*, 2021, **5**, 7384.
7 H. Zhang, X. Tan, H. Li, S. Passerini and W. Huang, *Energy Environ. Sci.*, 2021, **14**, 5788–5800.
8 M. Liu, H. Ao, Y. Jin, Z. Hou, X. Zhang, Y. Zhu and Y. Qian, *Mater. Today Energy*, 2020, **17**, 100432.
9 S. Boyd and V. Augustyn, *Inorg. Chem. Front.*, 2018, **5**, 999–1015.
10 D. Bin, F. Wang, A. G. Tamirat, L. Suo, Y. Wang, C. Wang and Y. Xia, *Adv. Energy Mater.*, 2018, **8**, 1703008.
11 C. Ding, Z. Chen, C. Cao, Y. Liu and Y. Gao, *Nano-Micro Lett.*, 2023, **15**, 192.
12 J. L. Sudworth, *J. Power Sources*, 1984, **11**, 143–154.
13 H. Li, X. Zhang, Z. Zhao, Z. Hu, X. Liu and G. Yu, *Energy Storage Mater.*, 2020, **26**, 83–104.
14 W. Tang, R. Qi, J. Wu, Y. Zuo, Y. Shi, R. Liu, W. Yan and J. Zhang, *Electrochem. Energy Rev.*, 2024, **7**, 23.
15 H. Zhu, F. Wang, L. Peng, T. Qin, F. Kang and C. Yang, *Angew. Chem., Int. Ed.*, 2022, **62**, e202212439.
16 J. Wang, Z. Wang, J. Ni and L. Li, *Energy Storage Mater.*, 2022, **45**, 704–719.
17 Y. Wu, W. Shuang, F. Chen, S. Tang, X. Wu, Z. Bai, L. Yang and J. Zhang, *Electrochem. Energy Rev.*, 2024, **7**, 17.
18 Z. Guo, Y. Zhao, Y. Ding, X. Dong, L. Chen, J. Cao, C. Wang, Y. Xia, H. Peng and Y. Wang, *Chem*, 2017, **3**, 348–362.
19 B. He, P. Man, Q. Zhang, C. Wang, Z. Zhou, C. Li, L. Wei and Y. Yao, *Small*, 2019, **15**, 1905115.
20 L. Yang, P. Wang, S. Zhang, Y. Wang, L. Zang, H. Zhu, J. Yin and H. Yang, *J. Mater. Chem. A*, 2020, **8**, 22791–22801.

21 B. He, K. Yin, W. Gong, Y. Xiong, Q. Zhang, J. Yang, Z. Wang, Z. Wang, M. Chen, P. Man, P. Coquet, Y. Yao, L. Sun and L. Wei, *Nano Energy*, 2021, **82**, 105764.
22 M. Kumar and T. C. Nagaiah, *Energy Storage Mater.*, 2022, **49**, 390–400.
23 Y. Zhao, J. He, L. Hu, J. Yang, C. Yan and M. Shi, *Small*, 2023, **19**, 2304182.
24 H. Ren, X. Zhang, Q. Liu, W. Tang, J. Liang and W. Wu, *Small*, 2024, **20**, 2312207.
25 F. Mo, G. Liang, Z. Huang, H. Li, D. Wang and C. Zhi, *Adv. Mater.*, 2019, **32**, 1902151.
26 B. Yao, J. Zhang, T. Kou, Y. Song, T. Liu and Y. Li, *Adv. Sci.*, 2017, **4**, 1700107.
27 S. Li, R. Dong, Y. Li, X. Lu, J. Qian, F. Wu, C. Wu and Y. Bai, *Mater. Today*, 2024, **72**, 207–234.
28 S. Jayakumar, P. C. Santhosh, M. M. Mohideen and A. V. Radhamani, *J. Alloys Compd.*, 2024, **976**, 173170.
29 J. Wang, F. Zheng, Y. Yu, P. Hu, M. Li, J. Wang, J. Fu, Q. Zhen, S. Bashir and J. Liu, *Chem. Eng. J.*, 2021, **426**, 131804.
30 P. Ragupathy, H. N. Vasan and N. Munichandraiah, *J. Electrochem. Soc.*, 2008, **155**, A34–A40.
31 Y. Liu, Y. Qiao, W. Zhang, H. Wang, K. Chen, H. Zhu, Z. Li and Y. Huang, *J. Mater. Chem. A*, 2015, **3**, 7780–7785.
32 L. Rakočević, S. Štrbac, J. Potočnik, M. Popović, D. Jugović and I. S. Simatović, *Ceram. Int.*, 2021, **47**, 4595–4603.
33 R. Chua, Y. Cai, Z. Kou, R. Satish, H. Ren, J. Chan, L. Zhang, S. A. Morris, J. Bai and M. Srinivasan, *Chem. Eng. J.*, 2019, **370**, 742–748.
34 X. Shan, F. Guo, D. S. Charles, Z. Lebens-Higgins, S. Abdel Razek, J. Wu, W. Xu, W. Yang, K. L. Page, J. C. Neuefeind, M. Feygenson, L. F. J. Piper and X. Teng, *Nat. Commun.*, 2019, **10**, 4975.
35 Z. Hao, X. Shi, Z. Yang, X. Zhou, L. Li, C. Ma and S. Chou, *Adv. Mater.*, 2024, **36**, 2305135.
36 M. Zheng, Z. Bai, Y. He, S. Wu, Y. Yang and Z. Zhu, *ACS Omega*, 2020, **5**, 5192–5201.
37 X. Cao, A. Pan, B. Yin, G. Fang, Y. Wang, X. Kong, T. Zhu, J. Zhou, G. Cao and S. Liang, *Nano Energy*, 2019, **60**, 312–323.
38 J. Peng, W. Zhang, Q. Liu, J. Wang, S. Chou, H. Liu and S. Dou, *Adv. Mater.*, 2022, **34**, 2108384.
39 Y. Xiao, J. Xiao, H. Zhao, J. Li, G. Zhang, D. Zhang, X. Guo, H. Gao, Y. Wang, J. Chen, G. Wang and H. Liu, *Small*, 2024, **20**, 2401957.
40 G. Du and H. Pang, *Energy Storage Mater.*, 2021, **36**, 387–408.
41 H. Yi, R. Qin, S. Ding, Y. Wang, S. Li, Q. Zhao and F. Pan, *Adv. Funct. Mater.*, 2020, **31**, 2006970.
42 Y. You, X. Wu, Y. Yin and Y. Guo, *Energy Environ. Sci.*, 2014, **7**, 1643–1647.
43 X. Lamprecht, F. Speck, P. Marzak, S. Cherevko and A. S. Bandarenka, *ACS Appl. Mater. Interfaces*, 2022, **14**, 3515–3525.
44 S. Jiao, J. Tuo, H. Xie, Z. Cai, S. Wang and J. Zhu, *Mater. Res. Bull.*, 2017, **86**, 194–200.
45 C. Xu, J. Peng, X. Liu, W. Lai, X. He, Z. Yang, J. Wang, Y. Qiao, L. Li and S. Chou, *Small Methods*, 2022, **6**, 2200404.
46 T. Shao, C. Li, C. Liu, W. Deng, W. Wang, M. Xue and R. Li, *J. Mater. Chem. A*, 2019, **7**, 1749–1755.
47 H. Gao, S. Xin, L. Xue and J. B. Goodenough, *Chem*, 2018, **4**, 833–844.
48 M. Zhong, L. Kong, N. Li, Y. Liu, J. Zhu and X. Bu, *Coord. Chem. Rev.*, 2019, **388**, 172–201.
49 X. Li, C. He, J. Zheng, W. Ye, W. Yin, B. Tang and Y. Rui, *J. Alloys Compd.*, 2020, **842**, 155605.
50 J. Jiang, Y. Jiang, Z. Chen, C. Tang, Y. Cheng, Q. Zhuang and Z. Ju, *Mater. Lett.*, 2023, **352**, 135092.
51 Q. Zhou, C. Xia, J. Li, A. Cheng, J. Liu, H. Liu, L. Li and S. Wang, *Solid State Ionics*, 2024, **411**, 116553.
52 Y. Liu, D. Liu, P. Liu, C. Liu and J. Zhou, *J. Colloid Interface Sci.*, 2024, **666**, 118–130.
53 L. Chen, Y. Li, X. Wang, J. Wu, Y. Ding, S. Ren, L. Zhang, Z. Xu, B. Chen, D. Han and Y. Wu, *Chem. Eng. J.*, 2023, **464**, 142658.
54 L. Wang, Y. Ni, X. Hou, L. Chen, F. Li and J. Chen, *Angew. Chem., Int. Ed.*, 2020, **59**, 22126–22131.
55 T. Jin, X. Ji, P. Wang, K. Zhu, J. Zhang, L. Cao, L. Chen, C. Cui, T. Deng, S. Liu, N. Piao, Y. Liu, C. Shen, K. Xie, L. Jiao and C. Wang, *Angew. Chem., Int. Ed.*, 2021, **60**, 11943–11948.
56 X. Wang, H. Huang, F. Zhou, P. Das, P. Wen, S. Zheng, P. Lu, Y. Yu and Z. Wu, *Nano Energy*, 2021, **82**, 105688.
57 X. Shen, M. Han, X. Li, P. Zhang, C. Yang, H. Liu, Y. Hu and J. Zhao, *ACS Appl. Mater. Interfaces*, 2022, **14**, 6841–6851.
58 L. Sharma, K. Nakamoto, R. Sakamoto, S. Okada and P. Barpanda, *ChemElectroChem*, 2018, **6**, 444–449.
59 H. Liu, W. Lei, Z. Tong, X. Li, Z. Wu, Q. Jia, S. Zhang and H. Zhang, *Adv. Mater. Interfaces*, 2020, **7**, 2000494.
60 Y. Zhang, L. Tao, C. Xie, D. Wang, Y. Zou, R. Chen, Y. Wang, C. Jia and S. Wang, *Adv. Mater.*, 2020, **32**, 1905923.
61 J. Wu, Y. Faiz, S. Hussain, F. Faiz, N. Zarshad, A. U. Rahman, M. A. Masood, Y. Deng, X. Pan and M. Ahmad, *Electrochim. Acta*, 2023, **443**, 141927.
62 M. S. Chae, A. Chakraborty, S. Kunnikuruvan, R. Attias, S. Maddukuri, Y. Gofer, D. T. Major and D. Aurbach, *Adv. Energy Mater.*, 2020, **10**, 2002077.
63 G. Chen, Q. Huang, T. Wu and L. Lu, *Adv. Funct. Mater.*, 2020, **30**, 2001289.
64 R. S. Kate, H. S. Jadhav, U. P. Chothe, K. Bhattacharjee, M. V. Kulkarni, R. J. Deokate, B. B. Kale and R. S. Kalubarme, *J. Mater. Chem. A*, 2024, **12**, 7418–7451.
65 X. Zhang, X. Rui, D. Chen, H. Tan, D. Yang, S. Huang and Y. Yu, *Nanoscale*, 2019, **11**, 2556–2576.
66 K. Wang, H. Li, G. Guo, L. Zheng, S. Passerini and H. Zhang, *ACS Energy Lett.*, 2023, **8**, 1671–1679.
67 B. Mai, B. Xing, Y. Yue, N. Cai, C. Cai, S. Lian, H. Fan, M. Yan, T. Zhu, P. Hu, X. Wang and L. Mai, *J. Mater. Sci. Technol.*, 2023, **165**, 1–7.
68 H. Yi, M. Ling, W. Xu, X. Li, Q. Zheng and H. Zhang, *Nano Energy*, 2018, **47**, 340–352.
69 X. Jiang, C. Liu, Q. Huang, W. Cao, Y. Chen and L. Guo, *J. Alloys Compd.*, 2022, **928**, 167119.

70 C. Guo, J. Yang, Z. Cui, S. Qi, Q. Peng, W. Sun, L. Lv, Y. Xu, Y. Wang and S. Chen, *J. Energy Chem.*, 2022, **65**, 514–523.
71 Z. Yang, G. Li, J. Sun, L. Xie, Y. Jiang, Y. Huang and S. Chen, *Energy Storage Mater.*, 2020, **25**, 724–730.
72 Y. Chen, X. Liao, P. Wang, J. Chen, X. Zhang, X. Wu, S. C. Smith, D. Lin, X. Tan and Q. Zheng, *J. Colloid Interface Sci.*, 2024, **653**, 1–10.
73 W. Liu, H. Yi, Q. Zheng, X. Li and H. Zhang, *J. Mater. Chem. A*, 2017, **5**, 10928–10935.
74 W. Song, X. Cao, Z. Wu, J. Chen, Y. Zhu, H. Hou, Q. Lan and X. Ji, *Langmuir*, 2014, **30**, 12438–12446.
75 T. Pan, Ruqia, C. Wu, C. Ni, S. Gull, A. Haider and H. Chen, *Electrochim. Acta*, 2022, **427**, 140778.
76 S. Ullah, A. Rehman, T. Najam, I. Hossain, S. Anjum, R. Ali, M. Shahid, S. Shah and M. Nazir, *J. Ind. Eng. Chem.*, 2024, **137**, 87–105.
77 Y. Yuan, D. Bin, X. Dong, Y. Wang, C. Wang and Y. Xia, *ACS Sustainable Chem. Eng.*, 2020, **8**, 3655–3663.
78 G. Yuan, J. Xiang, H. Jin, Y. Jin, L. Wu, Y. Zhang, A. Mentbayeva and Z. Bakenov, *Electrochim. Acta*, 2018, **259**, 647–654.
79 L. Shao, J. Hong, S. Wang, F. Wu, F. Yang, X. Shi and Z. Sun, *J. Power Sources*, 2021, **491**, 229627.
80 X. Yang and A. Rogach, *Adv. Energy Mater.*, 2020, **10**, 2000288.
81 Z. He, Y. Huang, H. Liu, Z. Geng, Y. Li, S. Li, W. Deng, G. Zou, H. Hou and X. Ji, *Nano Energy*, 2024, **129**, 109996.
82 D. Xiao, L. Zhang, Z. Li, H. Dou and X. Zhang, *Energy Storage Mater.*, 2022, **44**, 10–28.
83 Y. Niu, Y. Guo, Y. Yin, S. Zhang, T. Wang, P. Wang, S. Xin and Y. Guo, *Adv. Mater.*, 2020, **32**, 2001419.
84 S. Kandula, B. Sik Youn, J. Cho, H. K. Lim and J. Gon Son, *Chem. Eng. J.*, 2022, **439**, 135678.
85 D. Chen, X. Miao, J. Liu, J. Geng, L. Zhang, Z. Dai, H. Dong, J. Yang and H. Geng, *Chem. Eng. J.*, 2022, **446**, 136772.
86 Y. Wang, M. Li, Y. Zhang and N. Zhang, *Nano Res.*, 2024, **17**, 6038–6057.
87 Y. Zhu, Y. Wang, Y. Wang, T. Xu and P. Chang, *Carbon Energy*, 2022, **4**, 1182–1213.
88 Y. Chen, X. Li, K. Park, W. Lu, C. Wang, W. Xue, F. Yang, J. Zhou, L. Suo, T. Lin, H. Huang, J. Li and J. B. Goodenough, *Chem*, 2017, **3**, 152–163.
89 E. Wang, M. Chen, X. Guo, S. Chou, B. Zhong and S. Dou, *Small Methods*, 2019, **4**, 1900163.
90 B. Cho, H. Lim, H. N. Lee, Y. M. Park, H. Kim and H. J. Kim, *Surf. Coat. Technol.*, 2021, **407**, 126797.
91 M. Kumar, A. K. Padhan, D. Mandal and T. C. Nagaiah, *Energy Storage Mater.*, 2022, **45**, 1052–1061.
92 Z. Liu, Y. An, G. Pang, S. Dong, C. Xu, C. Mi and X. Zhang, *Chem. Eng. J.*, 2018, **353**, 814–823.
93 Y. Cao, Y. Liu, D. Zhao, X. Xia, L. Zhang, J. Zhang, H. Yang and Y. Xia, *ACS Sustainable Chem. Eng.*, 2020, **8**, 1380–1387.
94 X. Yan, Y. Zhou, W. Zhou, K. H. Lam and X. Hou, *Electrochim. Acta*, 2022, **429**, 140925.
95 Q. Meng, J. Shao, X. Dou and H. Chi, *Small*, 2024, **20**, 2308483.
96 G. Pang, P. Nie, C. Yuan, L. Shen, X. Zhang, J. Zhu and B. Ding, *Energy Technol.*, 2014, **2**, 705–712.
97 M. Kumar, N. Thakur, A. Bordoloi, A. Kumar Yadav, S. N. Jha, D. Bhattacharyya, D. Mandal and T. C. Nagaiah, *J. Mater. Chem. A*, 2022, **10**, 11394–11404.
98 Y. He, H. Chen, Y. Wang, Y. Zhang, L. Hou, R. Jiang and C. Yuan, *Electrochim. Acta*, 2023, **447**, 142128.
99 X. Yao, Y. Luo, Y. Li, W. Li, M. Fang, M. Shui, J. Shu and Y. Ren, *Mater. Res. Bull.*, 2018, **104**, 194–201.
100 Y. Qiu, Y. Yu, J. Xu, Y. Liu, M. Ou, S. Sun, P. Wei, Z. Deng, Y. Xu, C. Fang, Q. Li, J. Han and Y. Huang, *J. Mater. Chem. A*, 2019, **7**, 24953–24963.
101 J. Wu, L. Yang, H. Liu, H. Bu, W. Wang, C. Zeng and S. Zhu, *J. Appl. Electrochem.*, 2022, **52**, 1563–1572.
102 S. Liu, L. Wang, J. Liu, M. Zhou, Q. Nian, Y. Feng, Z. Tao and L. Shao, *J. Mater. Chem. A*, 2019, **7**, 248–256.
103 F. Malchik, N. Shpigel, M. D. Levi, T. R. Penki, B. Gavriel, G. Bergman, M. Turgeman, D. Aurbach and Y. Gogotsi, *Nano Energy*, 2021, **79**, 105433.
104 Y. Zhou, X. Shao, K. H. Lam, Y. Zheng, L. Zhao, K. Wang, J. Zhao, F. Chen and X. Hou, *ACS Appl. Mater. Interfaces*, 2020, **12**, 30328–30335.
105 T. Zhu, P. Hu, X. Wang, Z. Liu, W. Luo, K. A. Owusu, W. Cao, C. Shi, J. Li, L. Zhou and L. Mai, *Adv. Energy Mater.*, 2019, **9**, 1803436.
106 Y. Jiang, J. Shi, M. Wang, L. Zeng, L. Gu and Y. Yu, *ACS Appl. Mater. Interfaces*, 2015, **8**, 689–695.
107 J. Yang, H. Wang, P. Hu, J. Qi, L. Guo and L. Wang, *Small*, 2015, **11**, 3744–3749.
108 H. Gao and J. B. Goodenough, *Angew. Chem., Int. Ed.*, 2016, **55**, 12768–12772.
109 S. Qiu, X. Wu, M. Wang, M. Lucero, Y. Wang, J. Wang, Z. Yang, W. Xu, Q. Wang, M. Gu, J. Wen, Y. Huang, Z. Xu and Z. Feng, *Nano Energy*, 2019, **64**, 103941.
110 Z. Tian, Y. Zou, G. Liu, Y. Wang, J. Yin, J. Ming and H. N. Alshareef, *Adv. Sci.*, 2022, **9**, 2201207.
111 X. Li, X. Wang, L. Ma and W. Huang, *Adv. Energy Mater.*, 2022, **12**, 2202068.
112 H. Cheng, Q. Sun, L. Li, Y. Zou, Y. Wang, T. Cai, F. Zhao, G. Liu, Z. Ma, W. Wahyudi, Q. Li and J. Ming, *ACS Energy Lett.*, 2022, **7**, 490–513.
113 C. Li, H. Xu, L. Ni, B. Qin, Y. Ma, H. Jiang, G. Xu, J. Zhao and G. Cui, *Adv. Energy Mater.*, 2023, **13**, 2301758.
114 L. Suo, O. Borodin, Y. Wang, X. Rong, W. Sun, X. Fan, S. Xu, M. A. Schroeder, A. V. Cresce, F. Wang, C. Yang, Y. Hu, K. Xu and C. Wang, *Adv. Energy Mater.*, 2017, **7**, 1701189.
115 G. Plečkaitytė, M. Petrulevičienė, L. Staišiūnas, D. Tediashvili, J. Pilipavičius, J. Juodkazytė and L. Vilčiauskas, *J. Mater. Chem. A*, 2021, **9**, 12670–12683.
116 X. Zhao, Z. Xing and C. Huang, *J. Mater. Chem. A*, 2023, **11**, 22835–22844.
117 J. Kim, S. H. Yi, L. Li and S. E. Chun, *J. Energy Chem.*, 2022, **69**, 649–658.
118 R. Meija, V. Lazarenko, A. Skrastina, Y. Rublova, J. Andzane, V. Voikiva, A. Viksna and D. Erts, *Batteries*, 2022, **8**, 25.
119 X. Li, X. Zhu, J. Liang, Z. Hou, Y. Wang, N. Lin, Y. Zhu and Y. Qian, *J. Electrochem. Soc.*, 2014, **161**, A1181–A1187.

120 B. Zhang, Y. Liu, X. Wu, Y. Yang, Z. Chang, Z. Wen and Y. Wu, *Chem. Commun.*, 2014, **50**, 1209–1211.
121 T. Zhu, H. Kong, T. Xia, Y. Shen, Y. Miao and X. Zhao, *Mater. Res. Bull.*, 2021, **138**, 111209.
122 M. K. Ramos, G. Martins, L. H. Marcolino-Junior, M. F. Bergamini, M. M. Oliveira and A. J. G. Zarbin, *Mater. Horiz.*, 2023, **10**, 5521–5537.
123 Y. Wang, Z. Feng, D. Laul, W. Zhu, M. Provencher, M. L. Trudeau, A. Guerfi and K. Zaghib, *J. Power Sources*, 2018, **374**, 211–216.
124 S. H. Jeong, B. H. Kim, Y. D. Park, C. Y. Lee, J. Y. Mun and A. Tron, *J. Alloys Compd.*, 2019, **784**, 720–726.
125 J. Liu, C. Yang, B. Wen, B. Li and Y. Liu, *Small*, 2023, **19**, 2303896.
126 P. Marzak, P. Moser, S. Schreier, D. Scieszka, J. Yun, O. Schneider and A. S. Bandarenka, *Small Methods*, 2019, **3**, 1900445.
127 S. Zhang, C. Zhao, K. Zhu, J. Zhao, Y. Gao, K. Ye, J. Yan, G. Wang and D. Cao, *Energy Environ. Mater.*, 2022, **6**, e12388.
128 M. S. Chae, H. J. Kim, J. Lyoo, R. Attias, Y. Elias, Y. Gofer, S. T. Hong and D. Aurbach, *ACS Appl. Energy Mater.*, 2020, **3**, 10744–10751.
129 H. Ao, Y. Zhao, J. Zhou, W. Cai, X. Zhang, Y. Zhu and Y. Qian, *J. Mater. Chem. A*, 2019, **7**, 18708.
130 Y. Zhou, Z. Zhang, Y. Zhao, J. Liu, K. H. Lam, X. Zheng, H. Lou and X. Hou, *Chem. Eng. J.*, 2021, **425**, 130459.
131 H. Qin, Z. Song, H. Zhan and Y. Zhou, *J. Power Sources*, 2014, **249**, 367–372.
132 R. S. Kühnel, D. Reber and C. Battaglia, *ACS Energy Lett.*, 2017, **2**, 2005–2006.
133 L. Shen, H. Yang, Y. Jiang, J. Ma, T. Sun, M. Zhang and N. Zhu, *ACS Sustainable Chem. Eng.*, 2021, **9**, 3490–3497.
134 I. Ahmad and A. Kumar, *Chem. Eng. J.*, 2023, **477**, 146972.
135 M. S. Arsha and V. Biju, *J. Energy Storage*, 2023, **70**, 108064.
136 J. Han, A. Mariani, S. Passerini and A. Varzi, *Energy Environ. Sci.*, 2023, **16**, 1480–1501.
137 H. Wu, J. Hao, Y. Jiang, Y. Jiao, J. Liu, X. Xu, K. Davey, C. Wang and S. Qiao, *Nat. Commun.*, 2024, **15**, 575.
138 Y. Dong, H. Hu, P. Liang, L. Xue, X. Chai, F. Liu, M. Yu and F. Cheng, *Nat. Rev. Chem.*, 2025, **9**, 102–117.
139 Q. Nian, J. Wang, S. Liu, T. Sun, S. Zheng, Y. Zhang, Z. Tao and J. Chen, *Angew. Chem.*, 2019, **131**, 17150–17155.
140 Y. Sun, Y. Wang, L. Liu, B. Liu, Q. Zhang, D. Wu, H. Zhang and X. Yan, *J. Mater. Chem. A*, 2020, **8**, 17998–18006.
141 J. Hao, L. Yuan, C. Ye, D. Chao, K. Davey, Z. Guo and S. Qiao, *Angew. Chem., Int. Ed.*, 2021, **60**, 7366–7375.
142 K. Zhu, Z. Sun, Z. Li, P. Liu, X. Chen and L. Jiao, *Energy Storage Mater.*, 2022, **53**, 523–531.
143 N. Chang, T. Li, R. Li, S. Wang, Y. Yin, H. Zhang and X. Li, *Energy Environ. Sci.*, 2020, **13**, 3527–3535.
144 Y. Huang, J. Zhang, J. Liu, Z. Li, S. Jin, Z. Li, S. Zhang and H. Zhou, *Mater. Today Energy*, 2019, **14**, 100349.
145 L. Zhong, Y. Lu, H. Li, Z. Tao and J. Chen, *ACS Sustainable Chem. Eng.*, 2018, **6**, 7761–7768.
146 J. Zhang, C. Cui, P. Wang, Q. Li, L. Chen, F. Han, T. Jin, S. Liu, H. Choudhary, S. R. Raghavan, N. Eidson, A. V. Cresce, L. Ma, J. Uddin, D. Addison, C. Yang and C. Wang, *Energy Environ. Sci.*, 2020, **13**, 2878–2887.
147 Z. Wang, H. Li, Z. Tang, Z. Liu, Z. Ruan, L. Ma, Q. Yang, D. Wang and C. Zhi, *Adv. Funct. Mater.*, 2018, **28**, 180456.
148 T. Liu, X. Du, H. Wu, Y. Ren, J. Wang, H. Wang, Z. Chen, J. Zhao and G. Cui, *Angew. Chem., Int. Ed.*, 2023, **62**, e202311589.
149 Q. Gui, Y. Li and J. Liu, *J. Colloid Interface Sci.*, 2024, **662**, 119–128.
150 B. Dai, X. Shi, X. Pei, F. Xu and Y. Zhao, *Energy Storage Mater.*, 2024, **66**, 103231.
151 Z. Liu, Q. Yang, D. Wang, G. Liang, Y. Zhu, F. Mo, Z. Huang, X. Li, L. Ma, T. Tang, Z. Lu and C. Zhi, *Adv. Energy Mater.*, 2019, **9**, 1902473.
152 Z. Wang, Y. Li, J. Wang, R. Ji, H. Yuan, Y. Wang and H. Wang, *Carbon Energy*, 2022, **4**, 411–445.
153 X. Cao, L. Wang, J. Chen and J. Zheng, *J. Mater. Chem. A*, 2018, **6**, 15762–15770.
154 X. Wang, Z. Zhou, Z. Sun, J. Hah, Y. Yao, K. S. Moon, J. Di, Q. Li and C. P. Wong, *Nano-Micro Lett.*, 2020, **13**, 1–12.
155 C. Sun, Z. Han, X. Wang, B. Liu, Q. Li, H. Li, J. Xu, J. Cao and X. Wu, *Adv. Funct. Mater.*, 2023, **33**, 2305606.
156 D. Yu, H. Wang, J. Yang, Z. Niu, H. Lu, Y. Yang, L. Cheng and L. Guo, *ACS Appl. Mater. Interfaces*, 2017, **9**, 21298–21306.
157 Y. Zhou, Z. Wang and Y. Lu, *Mater. Today Energy*, 2021, **19**, 100570.
158 G. Tang, X. Zhang, B. Tian, P. Guo, J. Liang and W. Wu, *Chem. Eng. J.*, 2023, **471**, 144590.
159 J. Liang, B. Tian, X. Zhang, C. Jiang, D. He and W. Wu, *J. Mater. Chem. A*, 2023, **11**, 3493–3503.
160 B. Zhao, P. Jia, L. Yu, Y. Song, Z. Li, Y. Wang, R. Feng, H. Li, X. Cui, H. Cui, Y. Wang, M. Zhao, X. Zhao, X. Fang and Y. Pan, *J. Energy Storage*, 2023, **73**, 109174.
161 M. K. Shobana, *J. Alloys Compd.*, 2020, **831**, 154844.
162 J. Dong, G. Zhang, X. Wang, S. Zhang and C. Deng, *J. Mater. Chem. A*, 2017, **5**, 18725–18736.
163 S. Zhao, G. Li, Z. Li, K. Zhang, X. Chen, X. Dong, Y. Wang, Y. Cao and Y. Xia, *Adv. Funct. Mater.*, 2024, **18**, 2411007.